arXiv:astro-ph/0206042v1 4 Jun 2002

Structural Parameters for Globular Clusters in NGC 5128[1]

William E. Harris[2]

Department of Physics & Astronomy, McMaster University, Hamilton ON L8S 4M1

harris@physics.mcmaster.ca

Gretchen L. H. Harris[2]

Department of Physics, University of Waterloo, Waterloo ON N2L 3G1

glharris@astro.uwaterloo.ca

Stephen T. Holland

Department of Physics, University of Notre Dame, Notre Dame IN 46556-5670

sholland@nd.edu

and

Dean E. McLaughlin

Space Telescope Science Institute, 3700 San Martin Drive, Baltimore MD 21218

deanm@stsci.edu

ABSTRACT

We present new imaging measurements of 27 individual globular clusters in the halo of the nearby elliptical galaxy NGC 5128, obtained with the *Hubble Space Telescope* STIS and WFPC2 cameras. We use the cluster light profiles to determine their structural parameters (core and half-light radii, central concentration, and ellipticity). Combining these with similar data for selected inner-halo clusters from Holland et al. 1999 (AAp, 348, 418), we now have a total sample of 43 NGC 5128 globular clusters with measured structural properties. We find that classic King-model profiles match the clusters extremely well, and that their various structural parameters (core- and half-light radius,

[1]Based on observations with the NASA/ESA *Hubble Space Telescope*, obtained from the Space Telescope Science Institute, which is operated by the Association of Universities for Research in Astronomy (AURA), Inc., Under NASA Contract NAS 5-26555.

[2]Visiting Astronomer, Research School of Astronomy and Astrophysics, Australian National University, Weston ACT 2611, Australia

central surface brightness, central concentration) fall in very much the same range as do the clusters in the Milky Way and M31. We find half a dozen bright clusters which show tentative evidence for "extra-tidal light" that extends beyond the nominal tidal radius, similar in nature to several such objects previously found in the Milky Way and M31; these may represent clusters being tidally stripped, or possibly ones in which anisotropic velocity distributions are important. We also confirm previous indications that NGC 5128 contains relatively more clusters with large ($\epsilon > 0.2$) ellipticity than does the Milky Way. Instead, the $\epsilon-$distribution of the NGC 5128 clusters strongly resembles that of the old clusters in the LMC and also in M31. Finally, calculations of the cluster binding energies E_b as defined by McLaughlin 2000 (ApJ, 539,618) show that the NGC 5128 clusters occupy the same extremely narrow region of the parametric "fundamental plane" as do their Milky Way counterparts. Our data are thus strongly consistent with the claim that the globular clusters in both NGC 5128 and the Milky Way are fundamentally the same type of object: old star clusters with similar mass-to-light ratios and King-model structures.

Subject headings: galaxies: star clusters — galaxies: individual (NGC 5128)

1. Introduction

Globular star clusters have remarkably simple structures that are well approximated by isotropic, single-mass King (1966) models. In the multi-dimensional space of all their structural quantities such as scale radii, central concentration, surface brightness, velocity dispersion, mass-to-light ratio, and so forth, it is striking that real globular clusters in the Milky Way inhabit only a narrow region referred to as the fundamental plane (FP; see Djorgovski 1995).

Recently, McLaughlin (2000a) has shown that a particularly simple way of expressing the FP is to note that any King model is completely specified by four input parameters such as total cluster luminosity L, central concentration $c = \log\,(r_t/r_c)$, mass-to-light ratio, and binding energy E_b. Adding in the two strong empirical constraints that $M/L \simeq$ const and $E_b \sim L^2$ then requires the clusters to lie on a two-dimensional slice of this 4-space, leaving only two quantities (c and L) to determine the residual scatter on this FP. In turn, the concentration c is correlated with L, leaving the remarkable result that the structures of these clusters are fixed largely by just one major *internal* parameter, their total mass (or luminosity, at a given age). The *external* environment, i.e. its location in the Galactic tidal field, also has some influence on the FP parameters.

However, clusters may have formed under drastically different environmental conditions in other galactic environments (giant and dwarf ellipticals, starburst systems, galactic bulges and rings, etc.). The structures of clusters in these other types of galaxies remain to be investigated. The only other large galaxy for which this kind of study has been carried out in detail is M31, a large disk galaxy much like the Milky Way, and perhaps not surprisingly, its globular clusters

strongly resemble those of the Milky Way (Fusi Pecci et al. 1994; Holland et al. 1997; Barmby et al. 2002).

Beyond the Local Group, the nearest large galaxy containing many globular clusters available for detailed measurement is NGC 5128, the giant elliptical at the center of the Centaurus group at a distance $d \sim 4$ Mpc. More importantly, it is a very different type of galaxy than any in the Local Group, and quantitative study of its clusters holds considerable promise for adding constraints to formation modelling. In addition, a point of special interest from the viewpoint of globular cluster structural studies is that, because of sheer population size, NGC 5128 has many clusters at the upper end of the globular cluster mass distribution ($\gtrsim 10^6 M_\odot$); with a total population of perhaps 1900 clusters (G.Harris et al. 1984), it should have 40 to 50 clusters with $M_V \lesssim -10$. By contrast, all the Local Group galaxies combined contain perhaps ~ 600 globular clusters and thus have only a few with $M_V \lesssim -10$. NGC 5128 thus gives us the opportunity, in a single galaxy, to explore the empirical FP relations at extremely high cluster mass approaching $10^7 M_\odot$ ($M_V \sim -12$).

Clusters in galaxies as distant as Centaurus appear barely nonstellar under typical ground-based imaging resolutions of $1''$ but can be much more well resolved with the cameras on HST. The first clear demonstration that accurate structural profiles and King-model parameters could be obtained for these objects was provided by G.Harris et al. (1998), who studied a single outer-halo cluster in NGC 5128. Shortly afterward, Holland et al. (1999) obtained similar results for a selection of inner-halo clusters. In this paper, we present new imaging data for another sample of clusters in this important galaxy, more than doubling the total sample.

Throughout this paper we assume $d = 4.0$ Mpc for NGC 5128 and a foreground (Milky Way) reddening of $E_{B-V} = 0.11$, for an apparent distance modulus $(m - M)_V = 28.35$ (G.Harris et al. 2000). At this distance, 1 arcsecond is equivalent to a linear scale of 19.4 pc. Our adopted distance is a mean of the results from three methods including the red-giant-branch tip luminosity (G.Harris et al. 1999), the planetary nebula luminosity function (Hui et al. 1993), and the $I-$band surface brightness fluctuation technique (Tonry et al. 2001). The mean distance is likely to be uncertain to ± 0.2 Mpc based on the close mutual agreement of these methods.

2. Observational Material and Sample Definition

During the course of an HST Cycle 9 SNAPSHOT program (GO-8664) we obtained new images centered on 18 known globular clusters spread throughout the halo of NGC 5128. These were all 400-second exposures with the STIS camera in its unfiltered 50CCD/CL imaging mode and with gain=1 e^- per du. In addition to the STIS material, we also had in hand long-exposure WFPC2 (V, I) images (gain = 7) of four clusters from our previously published photometric studies of the halo red-giant stars in this galaxy (G.Harris et al. 1998; W.Harris & G.Harris 2002). Two objects, G302 and the newly discovered cluster C100 (see below), were imaged with both STIS and WFPC2, providing a small but useful consistency test of our structural fitting routines.

The candidate objects were all selected from the photometric list of known NGC 5128 clusters analyzed by G.Harris et al. (1992); our identification numbers (C and G prefixes) follow their list and are given in Table 1. All but one of our clusters were imaged either at the STIS scale of $0\farcs0507$/px or the PC1 scale of $0\farcs0455$/px; the one remaining object (G19) fell on the lower-resolution $0\farcs0996$/px scale of the WF3 camera.

All of the individual STIS and WFPC2 frames were inspected carefully to locate any clearly nonstellar objects in the field regardless of brightness, in addition to the previously known clusters. Almost two dozen additional cluster candidates not in any previous lists were located this way. On closer inspection, most of the "extra" candidates proved to be more likely to be faint background galaxies, with light profiles that were asymmetric, highly extended, or lumpy. However, seven were found to have characteristic sizes and symmetric King-type profiles like those of globular clusters and are thus kept in our sample. We believe these to be newly discovered clusters in NGC 5128. Our final list of 27 objects which we regard as definite or highly probable globular clusters in NGC 5128 is presented in Table 1; the seven new objects are assigned ID numbers C100 - C106.

In Figure 1, we show portions of the STIS images to illustrate the appearances of three of our measured clusters having a range of luminosities and galactocentric distances. As will be shown more quantitatively below, the cluster images are well resolved compared with the profiles of stars (PSFs).

3. Photometry

The first step in our analysis was to take the preprocessed images supplied by the STScI archive and derive positions and total magnitudes for each object. The coordinates were obtained directly from the information in the image headers and the STSDAS *xy2rd* routine and are expected to be accurate to $\pm 1''$. These are listed in columns (2) and (3) of Table 1, along with their projected galactocentric distance R_{gc} (column 3) under the assumption $d(\mathrm{NGC\ 5128}) = 4$ Mpc. The final column of the Table gives the particular detector (STIS, PC1, or WF3) on which the cluster was imaged.

For measurement of total magnitudes, we constructed curves of growth (integrated magnitude vs. aperture radius) from concentric-aperture photometry to select an aperture radius large enough to enclose almost all the cluster light without being dominated by sky noise. We adopted $r = 60$ px $\simeq 3''$ (as will be seen below, at this radius we reach the outermost extreme at which we can trace the surface brightness profile for most of the clusters). For a few cases where the objects were crowded by neighboring stars, we used the largest feasible uncrowded aperture radius and then applied the fiducial curves of growth to make the (small) necessary extrapolations out to $r = 3''$.

For the four clusters (C44, G19, G302, C100) on the WFPC2 frames, converting the integrated instrumental magnitudes into V and I was a straightforward matter of applying the usual calibration equations (Holtzman et al. 1995) for the relevant filters (F606W, F814W). Their resulting

$(V, V-I)$ magnitudes and colors are listed in columns (5) and (6) of Table 1.

For the much larger set of objects measured on STIS, the unfiltered ("clear" or CL) 50CCD configuration of the camera has a central wavelength near that of the standard V magnitude and thus can be transformed moderately well into V. Here we label the 50CCD "instrumental" magnitude as $v_{CL} \equiv -2.5 \log f_{CL}$ (where f_{CL} in DN/sec is the measured flux from the object). However, the zeropoints $(V - v_{CL})$ quoted in the literature (e.g. Rejkuba et al. 2000; Gardner et al. 2000), as well as the SYNPHOT method using PHOTFLAM from the image header, differ by 0.2 mag or more from one source to another. To set the STIS photometric zeropoint for this particular study we rely instead on two *local* calibration methods which employ the clusters themselves. Since these calibrating objects are exactly the same entities as our program objects, this approach also minimizes any systematic error due to nonzero color terms in the transformation. First, we used the small set of $(V, V-I)$ measurements for clusters obtained by Tonry & Schechter (1990); comparing our list with theirs revealed 11 clusters in common. Second, we used the Washington photometry (C, M, T_1) of the clusters published by G.Harris et al. (1992) along with the established conversion into V (see Geisler 1996),

$$V \;=\; T_1 \;+\; 0.052 \;+\; 0.256(C - T_1) \;. \qquad (1)$$

This approach gave V magnitudes for 16 clusters in our observed list.

In Figure 2 we plot the difference $(V - v_{CL})$ against V. The Tonry/Schechter sample gives $\langle V - v \rangle = 26.34 \pm 0.02$ with an rms dispersion ± 0.075 mag, while the transformed Washington photometry gives $\langle V - v \rangle = 26.27 \pm 0.02$ with dispersion ± 0.060 mag. Though there is a noticeable difference between the two methods, we have no basis to prefer one strongly over the other.[3] Averaging all the data together, we adopt $\langle V - v \rangle = 26.29 \pm 0.05$. In the end, it should be recognized that the STIS magnitudes cannot be as accurately calibrated as normal ones that are filter-defined, but they are expected to be useful to approximately the accuracy quoted. It is encouraging that, for our only uncrowded object measured with both WFPC2 and STIS (cluster G302), the calculated STIS/CL magnitude agrees with the WFPC2 one to 0.05 mag. The agreement is not as close for cluster C100, also measured with both STIS and PC1, but this object is severely crowded by a star of comparable brightness only $1''$ away.

4. Structural Parameters and Model Fitting

The model fitting was carried out in two partially independent ways as follows:

(1) We performed "two-dimensional" fits whereby a King (1966) model with a given set of parameters (W_0, r_c, c, ϵ) (central potential W_0, core radius r_c, central concentration $c = \log(r_t/r_c)$, and ellipticity $\epsilon = 1 - b/a$) is calculated, and then convolved with the full two-dimensional PSF shape

[3]From a more extensive comparison of the converted Washington photometry with the Tonry/Schechter sample, G.Harris et al. (1992) found a mean offset $\langle V_{TS} - V_W \rangle \simeq 0.04$ mag, very similar to our net difference of 0.07 ± 0.03.

for the given image. The PSF profile was determined empirically from several bright uncrowded stars on the frames. The seeing-convolved model is then matched to the surface brightness of the raw cluster image after subtraction of the background light, and the King model parameters are varied to achieve the best match to the data. The procedure is described fully in Holland et al. (1999).

(2) For comparison, we used the empirical ellipse-fitting code in *STSDAS* (*analysis.isophote.ellipse*) to generate smoothed profiles for all the candidate objects along with estimates of the surrounding local background light intensity. The *ellipse* code expects only that the light profile of the object is ellipsoidal and decreasing monotonically outward. In carrying out the fits we allowed the ellipticity and position angle of each annulus to vary but kept the ellipse center fixed. By subtracting the model from the original image and inspecting the residual light, we found that the background surface brightness b_V could be determined (on the STIS images) with a typical uncertainty of $e(b_V) \simeq 3$ DN (or $\pm 3e^-$ for a gain of 1 e^-/DN); changes in the background larger than that above or below the nominal b_V level left clearly distinct outer "edges" once the profile was subtracted from the cluster. In this way, we found that we could trace the cluster light profiles down to a level within about 3% - 5% of the sky background. Attempts to probe still fainter proved to push the measurements on these relatively short-exposure frames past their reliable limits. If higher S/N data are obtained in future, however, it should be possible to study the outermost envelopes of these clusters more thoroughly.

The *ellipse* code generated one-dimensional lists of surface brightness vs. semi-major axis. These were then matched to 1-D King model profiles convolved with the PSF profile. Sample profiles and best-fitting King models are shown in Figure 3 for four clusters covering a wide range of brightness. The seeing-convolved model profiles match the clusters quite well particularly in the inner and middle radial range where the cluster light is much brighter than the background. The only exceptions were a few of the very faintest objects for which the signal-to-noise was lowest and the contrast over background the smallest. Compared with the stellar PSF, which has a FWHM of $0\farcs11$, the cluster profiles are typically about three times broader and thus very well resolved.

Sample illustrations of the quality of fit of the generic King models are given in Figure 4, where (for the same four clusters as in Figure 3) we show the residuals after subtraction of the model profile from the *ellipse* code measurements. At an intensity level about one magnitude fainter than the background level, the internal uncertainties of the measured points become very large and do little to constrain the fit. At smaller radii, however, the model adheres closely to the data, with typical scatters of $\lesssim 0.05$ mag per data point. For comparison (see below), on these graphs the core radii of the clusters would fall typically at $\log r_c \sim -1.3$ and the half-light radii at $\log r_h \sim -0.4$, well within the higher-precision part of the fit.

In general we found that the two methods outlined above agreed well, though the 1-D fits tended to be numerically more robust (in several cases, particularly for faint objects, the 2-D fit did not converge satisfactorily). The adopted mean values of the structural parameters for all of

our program objects, from the average of the two methods, are summarized in Table 2. In the Table, we also include the half-light radius r_h as calculated from the model fit, since it is of interest as a quantity which is relatively immune to dynamical evolution within the cluster. The *projected* half-light radius R_h, a more conventionally used observational quantity, can be obtained from the (three-dimensional) quantity r_h by the numerical approximation $R_h \simeq 0.73 r_h$, which is accurate to a few percent over the range of $c-$values that apply to normal clusters.

The mean uncertainties in each measured quantity are listed at the bottom of the Table. Holland et al. (1999), through extensive numerical tests including simulated clusters, found that the expected measurement uncertainties for all quantities were 5% - 10% depending on brightness.

For the two clusters G302 and C100 (the latter object being crowded by a bright star, as noted above) measured on both the STIS and WFPC2 data, the independently determined model fits gave structural parameters in good mutual agreement (see Table 2). For these two, we adopted the core radii and ellipticities from the WFPC2 images since they were much longer exposures and thus higher S/N.

The central surface brightnesses μ_V^0 (V mag per arcsec^2) listed in Table 2 are partially "indirect" measurements in the sense that they are the surface brightnesses of our best-fit King-model curves read off at zero radius. We stress that the innermost core structures at $r << r_c$ cannot be truly resolved for any of our program objects. Thus (for example) if any of them is in fact a core-collapsed object with a power-law profile for the inner core, we would significantly underestimate μ_V^0 and overestimate r_c.

The last column of the Table gives the position angle θ of the isophotal major axis, measured counterclockwise (eastward) from North. The best-fitting orientation angle often varied by $\pm 20^o$ or so from the inner parts of the cluster to the outskirts, but our quoted mean refers to the position angle near the half-light radius r_h (see below). These orientation angles are more uncertain for clusters of smaller ellipticity. We find no statistical preference for any particular cluster orientation.

5. Clusters With Extratidal Light?

In the course of examining the profiles of all the individual clusters, we noted that for some of the brighter clusters in the sample, the fitted King models fell clearly below the measured cluster profile at the largest radii, even though the model fit was extremely accurate at smaller radii. In other words, within the context of the formal model fits (which are based on the assumptions of isotropic velocity dispersion and a single-mass stellar population) these clusters exhibit "extratidal light" (XTL) continuing outward past the nominal tidal radius r_t. Illustrations of this effect for four objects are shown in Figure 5. Although any individual data point at large radius is quite uncertain (see Fig. 4), these half-dozen clusters are among the brightest and have the best-determined profiles of the entire sample.

To test the reality of this phenomenon, we went through the numerical exercise of arbitrarily adjusting the adopted background intensity level b until the "extra" light at large radius essentially vanished and the residual outer profile approximately fit the King model at all radii. The size of this arbitrary shift Δb was then compared with the true external uncertainty in the background (typically $e_b \simeq \pm 3$ DN, as noted above). For most clusters in the sample, the necessary shift Δb was $\lesssim 2e_b$ and thus the significance of the effect was marginal at best; that is, we found that *small* positive or negative deviations relative to the King models at large radii could be readily understood as slightly incorrect adopted backgrounds. However, for six clusters (listed in Table 3), we found $\Delta b > 3e_b$ and for these we cautiously suggest the presence of a real XTL component.

All six of these clusters are brighter than $M_V = -10$ and thus are comparable with ω Centauri and NGC 6715, the two most luminous clusters in the Milky Way. For these six objects we subtracted the King model from the observed profile to derive the amount of residual light present in the XTL "tail". In Table 3, we list the projected galactocentric distance R_{gc}; the cluster luminosity M_V (including the XTL); the increase in background light Δb necessary to artificially remove the anomaly; and the fraction of the total cluster light which is in the extratidal component. Although they are only marginally significant, these fractions range from 7% to 17% of the cluster luminosity and thus represent a significant part of their entire stellar population. The candidate XTL objects show no preference for any particular halo location, with galactocentric distances ranging from 6 to 22 kpc.

The shapes of these extratidal profiles strongly resemble what has been found for a few clusters in both the Milky Way (Grillmair et al. 1995; Leon et al. 2000) and M31 (Grillmair et al. 1996). If the XTL is real, it may then represent tidally stripped or evaporated stars now drifting away from the cluster. Deeper imaging data than we have at present may be able to trace these faint components further outward along thin streamers which would mark out the clusters' orbital paths.

Another interpretation discussed in the recent literature (e.g. Lee et al. 1999; Majewski et al. 2000; Hughes & Wallerstein 2000; Carraro & Lia 2000; Hilker & Richtler 2000; Bekki et al. 2001; Meylan et al. 2001) is that objects like these may be the luminous, compact nuclei of former dwarf satellite galaxies (dE,N systems) that were accreted long ago. In this case, the XTL would be interpreted as the residual trace of the dE field-star population. This idea has gained additional impetus from the observation that NGC 6715 (the second most luminous cluster in the Milky Way halo) is near the center of the disrupting Sagittarius dwarf (e.g. Bassino & Muzzio 1995; Da Costa & Armandroff 1995; Layden & Sarajedini 2000) and also from a variety of recent observations of ω Cen indicating multi-epoch star formation (cf. the references cited above).

It is probably not surprising that several clusters in our sample (6 clusters out of 27 observed) show these extended envelopes, because our entire sample of clusters is biased in favor of such objects. As noted above, our candidates for STIS imaging were drawn from a list of known clusters (G.Harris et al. 1992) which were in turn identified from ground-based photographic plates on the basis of nonstellar appearance. Thus the objects in our list should be expected to be biased towards

bright clusters with extended envelopes which were easiest to pick out as nonstellar under $\simeq 1'' - 2''$ seeing. (One of the clusters we find to have an extended envelope, number C7, is the first cluster identified in NGC 5128 by Graham & Phillips 1980).

An alternative and more conservative interpretation of these extended profiles is that the outer parts of these clusters actually do not consist of "excess" light, but might be fitted instead by models incorporating multi-mass stellar populations and/or an anisotropic velocity distribution. Either or both of these steps would allow fitting of a greater range of projected density profiles (e.g. Gunn & Griffin 1979). Higher-quality data than we have at present will be needed to discriminate more clearly among these alternatives.

6. Structural Parameters and Correlations

The globular clusters we have observed in this program are scattered throughout the NGC 5128 halo, with projected galactocentric distances ranging from $\sim$ 6 to 25 kpc. Holland et al. (1999) have obtained structural parameters for 21 more objects projected on the *inner* halo of the galaxy ($R_{gc} < 3$ kpc), so by combining their sample with ours we can trace out any trends in the structural parameters over a much wider R_{gc} range.

From the Holland et al. list, we more or less arbitrarily reject five objects with extreme colors (4 with $V - I > 1.8$ which are likely to be either very heavily reddened globulars or background galaxies, and one very blue object with $V - I = 0.4$). All of these five have colors quite different from the $(V - I) \sim 1.0 \pm 0.2$ level characterizing all known globular clusters. The remaining 16, added to our 27, give a total list of 43 definite or highly probable globular clusters with measured King parameters. The major noteworthy difference between the two sets of objects is that the 16 from Holland et al. (1999) were all measured with rather short WFPC2 exposures (mostly 180 sec), with higher background light, and on the low-resolution WF2, 3 or 4 detectors. Thus they are taken from lower-S/N data and with poorer image sampling than were the majority of the objects in our new program.

6.1. Scale Radii

We first briefly compare our NGC 5128 clusters with those in the Milky Way, using data from the 1999 edition of the W.Harris (1996) catalog. As did Holland et al. (1999), we restrict the Milky Way sample to 78 clusters more luminous than $M_V \simeq -6.5$, with reddenings lower than $E_{B-V} = 1$, and further from the Galactic center than 1 kpc, to make it as similar as possible to our NGC 5128 sample. Histogram comparisons of core radius and ellipticity are shown in Figures 6 and 7.

The core radii for clusters in both galaxies fall very much in the same global range ($r_c \lesssim 4$ pc for almost all objects), and the medians of the two distributions are also similar (median $r_c = 1.01$ pc for

NGC 5128, 1.16 pc for the Milky Way). However, the Milky Way sample has relatively more objects at very small r_c. This difference is likely to be due to a combination of selection effects: as noted above, many of the NGC 5128 candidate clusters were pre-selected for their nonstellar appearance on ground-based images and thus the sample is already biased towards extended structure. In addition, it becomes increasingly difficult on numerical grounds to measure the true value of a core radius less than $0\farcs025$ (0.5 pc) given that it is convolved with a PSF profile with HWHM $\simeq 0\farcs05$. We suggest that there are likely to be many highly compact clusters with small core radii in NGC 5128 still waiting to be found.

Our NGC 5128 sample also lacks objects with *large* core radii $r_c \gtrsim 5$ pc, a few of which exist in the Milky Way comparison diagram. Although the current statistical sample is small, we believe that this discrepancy might well be due to selection effects as well. Most of these Milky Way objects are moderately faint, diffuse objects in the outer halo, and it is entirely likely that such objects would not have been noticed in the photographic image surveys from which our target list was selected (see above).

6.2. Ellipticities

Our cluster ellipticity measurements are shown in Figure 7 ($\epsilon = 1 - b/a$ where b/a is the minor-to-major axial ratio). These are weighted averages by annular luminosity over the measured radial range of the model fits and correspond roughly to the $\epsilon-$values at the "half-light" radius r_h commonly used in the literature. Often the fitted ellipticity is found to be a weak function of radius, though none of the clusters exhibited dramatic ellipticity gradients. In the second-last column of Table 2, we indicate whether the cluster showed a clear increase in ϵ with r (+), a decrease (−), or no significant gradient (blank column).

Returning to Figure 7, we note that NGC 5128 has a rather flat, or modestly declining, $\epsilon-$distribution over the range $0 < \epsilon < 0.3$.[4] From their small inner-halo sample of clusters, Holland et al. (1999) suggested that NGC 5128 had a much higher fraction of high-ellipticity clusters than did the Milky Way (White & Shawl 1987). We find that the medians for the two samples are at $\epsilon = 0.11$ for NGC 5128 and 0.05 for the Milky Way, and a standard K-S test shows that the two distributions differ significantly at higher than 99% confidence level. In short, we draw the same formal conclusion here as did Holland et al. However, we do not place excessive weight on it at this stage because of lingering uncertainties about possible selection effects in our samples, which

[4]The lack of NGC 5128 clusters at *very* small ellipticity $e < 0.04$ is likely to be an artifact of incomplete removal of the slightly elliptical PSF, as also noted by Holland et al. (1999). For larger ϵ, it is less clear whether or not any particular subtle biasses or selection effects may exist in our sample. The clusters were identified as members of NGC 5128 either on the basis of radial velocity, or on the basis of their nonstellar appearance from lower-resolution ground-based images in which their slightly out-of-round shapes would have been at least partly washed out. However, a much more complete candidate list will be needed before these issues can be addressed more securely.

still represent a very small fraction of the entire NGC 5128 cluster population (see the preceding footnote). In addition, the ellipticities for the Milky Way clusters follow from a somewhat different measurement process (see White & Shawl 1987) and the possibility of small systematic differences remains a concern.

The observed ellipticity must be a complex product of the initial structure of the cluster and its subsequent dynamical evolution but, as Meylan & Heggie (1997) comment, "our understanding of this problem is rather patchy". Flattening is almost certainly caused primarily by global rotation of the cluster rather than internal properties such as velocity anisotropy or external ones such as tidal elongation (Lagoute & Longaretti 1996; Meylan & Heggie 1997; Barmby et al. 2002). Recent dynamical models indicate that internal relaxation coupled to the external tidal field will in most cases drive a cluster towards rounder shape over several relaxation times t_{rh} (Fall & Frenk 1985; Lagoute & Longaretti 1996; Longaretti & Lagoute 1996; Einsel & Spurzem 1999). Evolution is generally faster at higher rotation, lower central potential W_0, or smaller galactocentric distance R_{gc}. Notable, but not overwhelming, evidence that this type of evolution actually occurs for real clusters may be seen in the LMC clusters, also shown in Fig. 7. The shaded part of the LMC histogram shows the $\epsilon-$distribution for 17 "old" clusters for which the evolutionary states should be more closely comparable with the Milky Way globulars (specifically, these 17 are in SWB age classes VI or VII). The unshaded part is for 48 younger clusters (data from Kontizas et al. 1989; Frenk & Fall 1982; Geisler & Hodge 1980). The median ellipticities are 0.12 ± 0.02 for the older clusters and 0.16 ± 0.01 for the younger ones (see also Frenk & Fall 1982, who argue for a similar trend).

The $\epsilon-$distribution for the LMC clusters has long been realized to be different from the Milky Way (Han & Ryden 1994; Kontizas et al. 1989, 1990; Bhatia & MacGillivray 1989; van den Bergh & Morbey 1984; Frenk & Fall 1982; Geisler & Hodge 1980, among others). Although an obvious problem with making such a comparison is that the great majority of the Magellanic objects are "young" ($T \lesssim 5$ Gyr) relative to the globulars in M31 and the Milky Way and thus less dynamically evolved, it appears to be true that Magellanic clusters of all ages have ϵ predominantly $\gtrsim 0.1$. Interestingly, the old-LMC group statistically resembles our NGC 5128 sample (they are different at less than 70% significance from a K-S test) much more closely than does the *younger* LMC group (which differs from NGC 5128 at more than 99% significance).

Lastly, in Figure 7 we also show comparisons with clusters in M31, where the data are drawn from the high-resolution HST-based imaging study of Barmby et al. (2002). For the M31 sample, we exclude four very faint objects with $\epsilon > 0.3$ to keep the same luminosity range $M_V \lesssim -6$ that we use for the Milky Way and NGC 5128. Even without these few high-ellipticity clusters, however, the NGC 5128 and M31 samples are also remarkably similar (the difference has less than 50% significance from a K-S test).

The M31/LMC/N5128 comparison casts some doubt on the hypotheses that either age or the strength of the external tidal field are the only, or major, factors determining the $\epsilon-$distributions:

instead, the data in these three quite different galaxies show that it is not unusual for very old clusters to have preserved clearly elliptical shapes ($\epsilon \gtrsim 0.2$) over a Hubble time and regardless of their present environment. Yet another recently found example of a luminous globular cluster with high ellipticity is object 13 in the lenticular galaxy NGC 1023, with $\epsilon \simeq 0.37$ (Larsen 2001). Of the four galaxies shown here, the Milky Way is the one which stands out as "different" from the other three. More comprehensive datasets (more galaxies, and more clusters per galaxy) will be needed to gain a better idea of the significance of this preliminary result.

In a previous paper (W.Harris & G.Harris 2001), we have noted that the metallicity distributions for the halo stars in NGC 5128, M31, and the LMC are also remarkably similar. The $\epsilon-$distributions may constitute additional evidence for our speculation that much of the stellar content of NGC 5128, and M31, formed within Magellanic-sized pregalactic units before assembling into the giant galaxies we see today.

6.3. Correlations with L and R_{gc}

In Figure 8, we show the central surface brightness of our clusters from Table 2, plotted against core radius r_c and central concentration c. Here, the μ_V^0 values have been corrected for foreground absorption, which we adopt as $A_V = 3.1E_{B-V} = 0.34$. Since our NGC 5128 sample is restricted mostly to the brighter ones in the galaxy, we are probing only a small part of the whole range of this correlation. Nevertheless, just as for the other cluster properties *except* possibly for the ellipticities (see above), the central surface brightnesses fall in the same broad regions of these scatter plots classically defined by the more well studied globular clusters in M31 and the Milky Way (shown in Figure 8 by the dashed lines, adapted from Figure 6 of Barmby et al. 2002). The scatter in the observed distribution arises from the spread in cluster luminosity L at a given r_c or μ^0 (see Figure 19 of McLaughlin 2000a and his accompanying discussion). The only notable exceptions are the two faintest objects in our set, C102 and C105, which have anomalously high central concentrations. However, the $c-$values for these faint objects are very uncertain, and the possibility remains that these two may be background galaxies which crept through our selection criteria. Higher-S/N images and multicolor measurements will be needed to confirm their identities.

In Figure 9 we show the scatter plots of core radius r_c, half-light radius r_h, central concentration index c, and ellipticity ϵ with cluster luminosity. The solid lines in each panel show the least-squares fits, which have the following slopes: $\Delta\log\, r_c/\Delta M_V = 0.02 \pm 0.03$, $\Delta\log\, r_h/\Delta M_V = 0.00 \pm 0.03$, $\Delta c/\Delta M_V = -0.07 \pm 0.04$, and $\Delta\epsilon/\Delta M_V = 0.02 \pm 0.01$. The scale radii r_c, r_h and ellipticity display considerable scatter and no significant trends with cluster luminosity, while the central concentration increases weakly with luminosity; weak correlations of r_c and c vs. luminosity were derived by McLaughlin (2000a) for the Milky Way clusters (shown in Figure 9 by the dashed lines). The lack of correlation of the characteristic radii r_c, r_h with luminosity is closely connected to the narrow distribution of clusters in the fundamental plane, which we discuss in the next section. Some of the r_c-distribution differences between the two galaxies are likely to be due simply to

the sample bias we noted above. For the $c(L)$ graph (lower left panel) we note that the higher-resolution, higher-S/N data (solid dots) follow the Milky Way relation much more closely than do the lower-resolution data (and would do so even more closely if the one "high" point at upper left were ignored, due to the very faint C102), suggesting perhaps that the $c-$values for the inner-halo data are systematically underestimated. The higher half-light radii from the lower-resolution data (upper right panel) may also be an artifact of the same effect. Higher-resolution data for more clusters will be needed before these concerns can be cleared up definitively.

In Figure 10 the same four quantities are plotted against projected galactocentric distance R_{gc}. The two subgroups of measured clusters (WFPC2 vs. STIS) are more clearly separated in Figure 10, because almost all of the lower-resolution WF data come from the inner-halo clusters. The same net offset towards lower c at smaller R_{gc} which we noted above is clearly visible in the lower left panel. Physically, we would have expected a higher mean c closer to the center of the galaxy because of the stronger effects of dynamical evolution, as well as a smaller mean r_h (see below), again indicating that the low WF resolution may have compromised the model fits for the inner clusters. On the other hand, any subtle real trends with R_{gc} may be washed out by the fact that we are observing only the projected distance rather than the true three-dimensional galactocentric distance.

As a further test of the effects of image resolution on the deduced structural parameters (see Holland et al. 1999, for a more extensive discussion including simulations), we carried out some brief numerical trials with the STIS data. For four clusters (C22, C23, C102, C103), we rebinned the original images down to 2× lower resolution ($0\farcs1$ per binned pixel) to roughly simulate the resolution of the WF camera. We then remeasured the cluster profiles and fit the 1-D King profiles as before. The results for the key structural parameters (W_0, c, r_c, r_h) were then compared with the original profiles. C23 is among the brightest in our sample, while C22 and C103 are of intermediate brightness and C102 is among the faintest. For the three brightest, the fitted W_0 values agreed with their higher-resolution counterparts to within 5%. The r_c and c values tended to be overestimated on the low-resolution images by about 5%-10%, while r_h was overestimated by about 20%. For the very faint C102, the agreement with the high-resolution parameters was no better than ±50%. These trials suggest to us that the 2× lower resolution by itself does not seriously damage the ability to measure the structural parameters (which at best are internally uncertain at the 10% level; see above). Instead, the signal-to-noise level of the data (exposure time, cluster luminosity, background light) seems to be a more important factor at the levels we are dealing with, and as noted above, the Holland et al. (1999) WFPC2 data were taken with shorter exposure times and higher background light from the inner halo.

6.4. Metallicity and Characteristic Cluster Size

Finally, in Figure 11 we show the scatter plot of cluster half-light radius versus measured metallicity. Since r_h is closely related to the half-mass radius r_{hm}, which remains relatively constant

over long timescales of dynamical evolution, r_h represents a useful characteristic scale size for the cluster. A formal least-squares solution gives $r_h(\mathrm{arcsec}) = (0.381 \pm 0.010) + (0.064 \pm 0.067)$ [Fe/H], confirming the immediate visual impression that no significant correlation exists. Dividing the sample more or less arbitrarily into metal-poor ([Fe/H] < -1) and metal-rich ([Fe/H] > -1) groups, we find that the mean characteristic radii $\langle r_h \rangle$ are (7.37 ± 1.03) pc and (7.14 ± 0.76) pc, indistinguishably different.

This result is formally at odds with what has been found for the M31 clusters (Barmby et al. 2002) and for the clusters in certain giant E galaxies (Kundu et al. 1999; Larsen et al. 2001b) and in the giant Sa galaxy M104 (Larsen et al. 2001b), where mild systematic *decreases* in cluster size with increasing metallicity have been claimed to exist. Our result, however, may be a simple consequence of working with a small sample which is selection-biased towards large clusters. A much more comprehensive imaging set will be needed to explore this potentially important correlation adequately.

7. Binding Energy and the Fundamental Plane

Djorgovski (1995) demonstrated that in the trivariate space of central surface brightness, velocity dispersion, and core radius, the Milky Way globular clusters occupy only a relatively narrow region now called the "fundamental plane", similar to that expected if the cores were virialized structures. Barmby et al. (2002) have shown definitively with a comparably large sample of M31 clusters that they too fall in very much the same restricted region of parameter space. Lacking any extensive direct measures of the internal velocity dispersions for the NGC 5128 clusters, we cannot define the same graphs as for the Milky Way and M31. We have, however, carried out a series of consistency tests which strongly suggest to us that the clusters in this giant E galaxy define a closely similar FP.

Here we cast the discussion in the way laid out by McLaughlin (2000a), in terms of the cluster *binding energies* E_b. The binding energy is fundamentally related to the cluster *mass* M, and on basic virial-theorem grounds, we expect a dependence of the form $E_b \sim f(c) \cdot M^2/r_c$. Combining McLaughlin's equations (A6) and (A7), we obtain E_b in terms of the cluster core radius, luminosity, central concentration, and mass-to-light ratio:

$$E_b \;=\; G\Big(\frac{4\pi}{9}\Upsilon\Big)^2 \frac{L^2}{r_c}\,\frac{\mathcal{E}(c)}{\mathcal{L}(c)^2} \tag{2}$$

where $\mathcal{E}, \mathcal{L}$ are dimensionless functions of c, and Υ is the mass-to-light ratio.

Independent calibrations of Υ require direct spectroscopic measurements of their internal velocity dispersions σ_v. As yet, little such material is available for NGC 5128 by comparison with the Milky Way and M31. Velocity dispersion measurements for 10 of the brightest NGC 5128 clusters are described by Dubath (1994) and stated to be in the range $15 - 25$ km s^{-1}. A subsequent discussion by Dubath & Grillmair (1997) uses these to show that the NGC 5128 clusters fall, within the

measurement uncertainties, on the top end of the same FP as in the Milky Way and M31. The list of measured velocities from Dubath (private communication, and in preparation) shows that there are four clusters in common between his sample and ours, and for these we can carry out complete calculations of Υ_V. These four objects are listed in Table 4. We combine McLaughlin's (2000a) expression (A1) defining Υ with his equation (A6) to eliminate the central luminosity density j_0, giving the mass-to-light ratio in terms of our measured parameters,

$$\Upsilon \;=\; \frac{9\mathcal{L}(c)\,\sigma_0^2\,r_c}{4\pi G L} \tag{3}$$

where the scale velocity σ_0 is given as a ratio of the measured dispersion σ_v by McLaughlin's relation (B1); for any $c-$values in our range of interest, we have $\sigma_0 \simeq \sigma_v$ to within a few percent. The structure of the cluster (particularly, its central concentration c) enters through the dimensionless function $\mathcal{L}$. Since $\mathcal{L}$ varies by more than a factor of 20 over the $c-$range occupied by typical globular clusters, Υ is quite sensitive to both the velocity dispersion and the cluster structure; we need to know both to estimate the cluster masses correctly.

Table 4 lists the measured velocity dispersions from Dubath; the structural luminosity parameter $\mathcal{L}$; and the calculated mass-to-light ratio Υ_V. Taking into account the measurement uncertainties in σ_v, c, r_c, the integrated V magnitudes, and the galaxy distance itself, we find that Υ is uncertain to $\pm 30\%$ for a given object. The weighted average over the four clusters is $\langle \Upsilon_V \rangle = 1.56 \pm 0.24$. By comparison, McLaughlin's mean value $\langle \Upsilon_V \rangle = 1.45 \pm 0.1$ (a mean over 39 Milky Way clusters) is not significantly different, and provides an encouraging consistency test that the two groups of clusters are similar.

If we now *assume* $\Upsilon_V = 1.45$ (the more precise Milky Way mean) then numerically Eq. (2) becomes

$$\log E_b\,(\mathrm{ergs}) \;=\; 41.545 \;+\; 2\log(L/L_\odot) \;-\; \log(r_c/\mathrm{pc}) \;+\; \log\mathcal{E}(c) \;-\; 2\log\mathcal{L}(c)\,. \tag{4}$$

Given (L, r_c, c) for each cluster we can then estimate its binding energy *modulo* our uncertainty in the mass-to-light ratio.

The results for our combined sample of 43 clusters are displayed graphically in Figure 12 as E_b versus L. A straightforward linear least-squares correlation, unweighted, gives

$$\log E_b\,(\mathrm{ergs}) \;=\; (40.41 \pm 0.40) \;+\; (1.952 \pm 0.070)\log\,(L/L_\odot)\ (\mathrm{NGC\ 5128}) \tag{5}$$

with a residual scatter in $\log E_b$ of ± 0.22 dex. The measurement uncertainties in the quantities used to calculate E_b generate expected scatters of ± 0.04 in $\log r_c$, ± 0.08 in $\log \mathcal{E}$, and ± 0.09 in $\log \mathcal{L}$. Adding these in quadrature, we obtain a net expected dispersion of ± 0.20 in $\log E_b$, sufficient to explain almost all of the observed spread in Figure 12.

For comparison, from a sample of 109 non-core-collapsed Milky Way clusters McLaughlin (2000a) obtained the correlation (see his Figure 6 and accompanying text)

$$\log E_b\,(\mathrm{ergs}) \;=\; (39.89 \pm 0.38) \;+\; (2.05 \pm 0.08)\log\,(L/L_\odot)\ (\mathrm{Milky\ Way}). \tag{6}$$

The dispersion about this latter relation is ±0.53 dex, though it should be noted that the scatter is ∼30% smaller if E_b is normalized to a constant Galactocentric distance; see the discussion of McLaughlin and his Figure 12.

A basic L^2 proportionality of E_b is of course built directly into Eq. (2). What is more interesting is that the observed slope of the actual sequence is so close to 2.00, and the scatter around the relation is so small, that the other factors $(r_c, \Upsilon, \mathcal{L}, \mathcal{E})$ *in combination* must not vary importantly with cluster mass M itself (see McLaughlin 2000a; Barmby et al. 2002, for more extensive discussion). Secondly, the NGC 5128 sequence falls along a locus which, within its own uncertainties, is indistinguishable from the Milky Way sequence, consistent with the claim that we are looking at very much the same type of object with the same mean mass-to-light ratio (see below).

The NGC 5128 results also demonstrate clearly that the $E_b(L)$ relation continues upward along the same slope to significantly higher cluster luminosities (masses) than were previously observed. Whereas the Milky Way has only two clusters more luminous than $M_V = -10$, our NGC 5128 sample has 14, and the relation now extends to almost a factor of three higher, reaching an equivalent mass of $4 \times 10^6 M_\odot$ for $\Upsilon = 1.45$.

Small though it is, some of the residual scatter in Figure 12 may correlate with other external factors such as age, metallicity, or galactocentric distance. Although we cannot evaluate age directly at present, the residual correlations against distance and metallicity are shown in Figure 13. To check for metallicity effects, we use 16 clusters in our list for which [Fe/H] values are known from the Washington photometry by G.Harris et al. (1992). Although $(V-I)$ colors are available for the other clusters in the list, most of these are inner-halo objects where some of the $(V-I)$ values are confused with possible internal reddening differences and are, in any event, not very sensitive to metallicity (see Holland et al. 1999). The resulting correlation (lower panel of Figure 13) is Δ log $(E_b/L^2)/\Delta$ [Fe/H] $= (0.00 \pm 0.07)$. Just as for the Milky Way, we find no trace of any dependence of binding energy on metallicity.

On the other hand, a change in mean E_b with galactocentric distance is expected. We have $E_b \sim M^2/r_{hm}$ by definition, and at least for the Milky Way, the characteristic cluster size r_{hm} is known to vary with R_{gc}. McLaughlin (2000a) finds empirically that $r_{hm} \sim R_{gc}^{0.4}$ for the Milky Way system, consistent with rough theoretical arguments that predict $r_{hm} \sim R_{gc}^{0.5}$ (e.g. W.Harris & Pudritz 1994) for an isothermal halo potential well. That is, the linear scale sizes of the clusters should reflect the sizes of their initial protocluster gas clouds, and the clouds will have larger scale sizes in the outer regions of the halo where they are under lower ambient pressures. In the NGC 5128 data sample we can look for the same effect, although (unlike the Milky Way) we can work only with the *projected* galactocentric distances rather than the full three-dimensional R_{gc}. In the upper panel of Figure 13 we show (E_b/L^2) versus R_{gc}, where the latter now denotes the projected distance. The resulting correlation is Δ log $(E_b/L^2)/\Delta$ log $R_{gc} = (-0.325 \pm 0.069)$. This is a significant trend in the same sense as was found for the Milky Way, though projection into two

dimensions has, as expected, left a shallower slope.[5]

Too much reliance cannot be placed on this latter result, since the datapoints at small R_{gc} may have measurement biasses as discussed above. Nevertheless, if we now rather boldly accept the main trend of the effect and normalize all the E_b values to a fiducial distance (10 kpc) by defining

$$E_b^\star \;=\; E_b \cdot (R_{gc}/10)^{0.325} \;, \tag{7}$$

the net result is to yield a corrected binding-energy relation as shown in Figure 14 with the equation

$$E_b^\star \;=\; (40.07 \pm 0.32) \;+\; (2.00 \pm 0.06)\log(L/L_\odot) \tag{8}$$

and with a dispersion of only ± 0.18 dex over its entire run.

The analysis so far has assumed a uniform age for all clusters in the sample. Age differences would be expected to enter mainly through the mass-to-light ratio, which decreases with increasing age. Since $E_b(L) \sim \Upsilon^2$, any mean age difference between the Milky Way and NGC 5128 would then show up in Figure 12 as a net offset of the data points away from the Milky Way line. If, for example, the NGC 5128 clusters were actually much younger, the points in Figure 14 would then have fallen above the Milky Way line: that is, by adopting the mean $\Upsilon = 1.45$ valid for old clusters, we would have overestimated their masses (and thus their binding energies) for a given luminosity. Approximate predictions for the amount of the effect are shown in Figure 14 by the two dotted lines parallel to the main relation, the upper one for a cluster age of 2 Gy and the lower one for 5 Gy. We have used Bruzual/Charlot relations (quoted by Whitmore et al. 1997) for the change in cluster luminosity ΔM_V with age to estimate these offsets. Thus for *individual* clusters, age differences of factors of two are discernible on this diagnostic graph. In practice, no offset from the Milky Way cluster line is detectable to well within the observational scatter, so our data are strongly consistent with the claim that we are looking at basically the same type of object in both galaxies: old, luminous star clusters with similar mass-to-light ratios.

McLaughlin (2000a,b) has suggested that the three quantities $(L, E_b^\star, c)$ provide a physically transparent way to describe the fundamental plane or "$\epsilon-$space" for globular cluster structures. In Figure 14 we are essentially looking at the FP edge-on, but tilted. A rectified form of the FP can be generated from a suitable rotation of the $(L, E_b^\star)$ plane, given by $\epsilon_1 \equiv \log\, E_b^\star - 2\, \log\, L$, $\epsilon_2 \equiv 2.00 \log E_b^\star + \log L$, and $\epsilon_3 \equiv c$. The edge-on view (Figure 14) is essentially a rotated version

[5]We note in passing that the trend shown in Figure 13, when it is extended to a larger and more well determined statistical sample, may eventually place some interesting new constraints on the formation history of NGC 5128. The reason is that the clusters which are *now* in the halo have characteristic radii r_{hm} that still reflect their place of formation. For example, if they formed within disks of large progenitor galaxies under conditions of high ambient pressure, they would maintain their original small characteristic sizes even after the disks merged to produce NGC 5128 and projected much of their material well out into the halo. On the other hand, if the clusters formed within lower-mass dwarfs which later merged, they would have larger effective radii consistent with the weak potential wells in which they formed. Detailed simulations will be needed to test whether the slope of a relation such as in Figure 13 can be maintained after a long series of mergers of many types of progenitor galaxies.

of (ϵ_1, ϵ_2). A fully "face-on" view of the FP can then be constructed from a plot of ϵ_2 against ϵ_3. This plot is shown in Figure 15. There is little left in this plane but pure scatter, but this may simply be reflecting the limitations of our small sample. A larger sample extending downward to much lower luminosities might reveal the same overall trend with c (lower central concentration at lower luminosity) that is clearly found in the Milky Way (compare Figure 13 of McLaughlin 2000a, shown here as the dashed line).

The remarkably tight $E_b(L)$ relation, for clusters at all galactocentric distances, hints that it was set largely by the cluster formation process (McLaughlin 2000a,b). For protocluster gas clouds E_b should behave in proportion to $M^{1.5}R_{gc}^{-0.5}$, if they are constrained at the time of star formation by an external pressure P_s which itself varies as $P_s \sim R_{gc}^{-2}$ in the isothermal potential well of the protogalaxy (see McLaughlin 2000b; W.Harris & Pudritz 1994). McLaughlin (2000b) gives the expected dependence of E_b(gas cloud) for the case of the Milky Way halo with circular velocity $V_c = 220$ km s^{-1}. Renormalizing to NGC 5128 with $V_c = 245$ km s^{-1} (Hui et al. 1995), we find under the same assumptions $E_b(\mathrm{gas}) \simeq 4.76 \times 10^{42}$ erg $\cdot M^{1.5} \cdot (R_{gc}/10\mathrm{kpc})^{-0.5}$. The location of this line, for $R = 10$ kpc and $(M/L) = 1.45$ as before, is shown in Figure 14. The fully formed clusters we observe today obey a distinctly different and steeper relation ($E_b \sim M^2$ rather than $M^{1.5}$), indicating perhaps that the lower-mass clusters lost relatively more of their binding energy through early gas loss.

Under the assumptions of this doubtless-oversimplified model, the protocluster E_b line should represent an upper boundary which could only be reached by the actual star clusters if their star formation efficiency approached 100%. However, we see that at the upper end the most massive known clusters lie *above* the gas-cloud relation by as much as a factor of two. At this point we can only speculate on possible interpretations: our schematic model for the gas clouds may be too rough, or the clusters may have evolved dynamically away from their initial conditions to a state of higher binding energy. The dynamics of cloud collapse and star formation during a cluster's earliest stages are poorly understood, and there may be various mass-dependent phenomena at work whose results we see in the present-day $E_b(L)$ correlation.

8. Summary

We have used new imaging data from the HST STIS and WFPC2 cameras to derive structural parameters for globular clusters in the halo of the giant elliptical galaxy NGC 5128. We find that classic, single-mass King models describe their observed light profiles extremely well, allowing us to derive parameters $(r_c, r_h, c, \epsilon, L)$ for direct comparison with the globular clusters in other galaxies. The NGC 5128 clusters occupy very much the same regions of parameter space as those in the Milky Way, with the exception that they have a higher range of ellipticities: they occupy the range $0 < \epsilon < 0.3$ more or less uniformly, and among various comparison galaxies within the Local Group, we find that they most nearly resemble the old clusters in the LMC and M31 in this respect. We also find half a dozen luminous clusters which may have "extratidal light" which is possibly due to

active tidal stripping or residual field-star populations from disrupted dwarf satellite galaxies, but may also be the signature of anisotropic velocity distributions.

Lastly, we find that the NGC 5128 clusters delineate a relation between binding energy E_b and luminosity L which is even tighter than in the Milky Way and in exactly the same region of the "fundamental plane". This work provides additional evidence that globular cluster formation processes were remarkably similar in galaxies of very different types.

Considerable further progress can be made in understanding the structures of clusters in this keystone galaxy if we can obtain a more extensive sample of objects over a wide range of galactocentric distances and at the highest resolution possible. In addition, direct spectroscopic measurements of their velocity dispersions are needed to check the key assumptions we have made about their mass-to-light ratios.

This work was supported by the Natural Sciences and Engineering Research Council of Canada through research grants to the authors. WEH and GLHH are pleased to acknowledge the hospitality and support at Mount Stromlo Observatory (RSAA/ANU) during research leaves when this paper was written. STH acknowledges support from NASA grant NAG5-9364. An anonymous referee provided several constructive suggestions which improved the manuscript. We also thank Georges Meylan for a helpful comment about the applicability of anisotropic velocity distributions. Finally, we are extremely grateful to Pierre Dubath for transmitting his cluster velocity dispersion data in advance of publication, allowing us to make crucial consistency checks on the mass-to-light ratios.

REFERENCES

Barmby, P., Holland, S.T., & Huchra, J.P. 2002, AJ, 123, 1937

Bassino, L.P., & Muzzio, J.C. 1995, Observatory, 115, 256

Bekki, K., Couch, W.J., & Drinkwater, M.J. 2001, ApJ, 552, L105

Bhatia, R.K., & MacGillivray, H.T. 1989, A&A, 211, 9

Carraro, G., & Lia, C. 2000, A&A, 357, 977

Da Costa, G.S., & Armandroff, T.E. 1995, AJ, 109, 2533

Djorgovski, S. 1995, ApJ, 438, L29

Einsel, C., & Spurzem, R. 1999, MNRAS, 302, 81

Dubath, P. 1994, Bull.AAS, 185, 5203

Dubath, P. 1997, A&A, 321, 379

Fall, S.M., & Frenk, C.S. 1985, in Dynamics of Star Clusters, IAU Symposium 113, ed. J.Goodman & P.Hut (Dordrecht: Reidel), p.285

Frenk, C.S., & Fall, S.M. 1982, MNRAS, 199, 565

Fusi Pecci, F. et al. 1994, A&A, 284, 349

Gardner, J.P. et al., 2000, AJ, 119, 486

Geisler, D. 1996, AJ, 111, 480

Geisler, D., & Hodge, P. 1980, ApJ, 242, 66

Graham, J.A., & Phillips, M.M. 1980, ApJ, 239, L97

Grillmair, C.J., Freeman, K.C., Irwin. M.J., & Quinn, P.J. 1995, AJ, 109, 2553

Grillmair, C.J., et al., 1996, AJ, 111, 2293

Gunn, J.E., & Griffin, R.F. 1979, AJ, 84, 752

Han, C., & Ryden, B.S. 1994, ApJ, 433, 80

Harris, G.L.H., Geisler, D., Harris, H.C., & Hesser, J.E. 1992, AJ, 104, 613

Harris, G.L.H., Hesser, J.E., Harris, H.C., & Curry, P.J. 1984, ApJ, 287, 175

Harris, G.L.H., Poole, G.B., & Harris, W.E. 1998, AJ, 116, 2866

Harris, G.L.H., Harris, W.E., & Poole, G.B. 1999, AJ, 117, 855

Harris, G.L.H., & Harris, W.E. 2000, AJ, 120, 2423

Harris, W.E. 1996, AJ, 112, 1487

Harris, W.E. 2001, in Star Clusters, Saas-Fee Advanced Course 28 (New York: Springer), ed. L.Labhardt & B.Binggeli.

Harris, W.E., & Harris, G.L.H. 2001, AJ, 122, 3065

Harris, W.E., & Harris, G.L.H. 2002, AJ, 123, in press

Harris, W.E., & Pudritz, R.E. 1994, ApJ, 429, 177

Hilker, M., & Richtler, T. 2000, A&A, 362, 895

Holland, S., Fahlman, G.G., & Richer, H.B. 1997, AJ, 114, 1488

Holland, S., Côté, P., & Hesser, J.E. 1999, A&A, 348, 418

Holtzman, J. A. et al. 1995, PASP, 107, 1065

Hughes, J., & Wallerstein, G. 2000, AJ, 119, 1225

Hui, X., Ford, H.C., Ciardullo, R., & Jacoby, G.H. 1993, ApJ, 414, 463

Hui, X., Ford, H.C., Freeman, K.C., & Dopita, M.A. 1995, ApJ, 449, 592

King, I.R. 1966, AJ, 71, 64

Kontizas, E., Kontizas, M., Sedmak, G., & Smareglia, R. 1989, AJ, 98, 590

Kontizas, E., Kontizas, M., Sedmak, G., Smareglia, R., & Dapergolas, A. 1990, AJ, 100, 425

Kundu, A., Whitmore, B.C., Sparks, W.B., Macchetto, F.D., Zepf, S.E., & Ashman, K.M. 1999, ApJ, 513, 733

Lagoute, C., & Longaretti, P.-Y. 1996, A&A, 308, 441

Larsen, S.S. 2001, AJ, 122, 1782

Larsen, S.S., Brodie, J.P., Huchra, J.P., Forbes, D.A., & Grillmair, C.J. 2001, AJ, 121, 2974

Larsen, S.S., Forbes, D.A., & Brodie, J.P. 2001, MNRAS, 327, 1116

Leon, S., Meylan, G., & Combes, F. 2000, A&A, 359, 907

Longaretti, P.-Y., & Lagoute, C. 1996, A&A, 308, 453

Layden, A.C., & Sarajedini, A. 2000, AJ, 119, 1760

Lee, Y.-W., Joo, J.-M., Sohn, Y.-J., Rey, S.-C., Lee, H.-C., & Walker, A.R. 1999, Nature, 402, 55

Majewski, S.R. et al. 2000, in The Galactic Halo: From Globular Clusters to Field Stars, 35th Liege International Astrophysics Colloquium, ed. A.Noels, P.Magain, D. Caro, E.Jehin, G.Parmentier, & A.A.Thoul (Liege: Institut d'Astrophysique et de Geophysique), p.619

McLaughlin, D.E. 2000a, ApJ,539, 618

McLaughlin, D.E. 2000b, in Massive Stellar Clusters, ASP Conference Series vol. 211, ed. A.Lancon & C.Boily (San Francisco: ASP), p.281

Meylan, G., & Heggie, D.C. 1997 A&A Rev., 8, 1

Meylan, G., Sarajedini, A., Jablonka, P., Djorgovski, S.G., Bridges, T., & Rich, R.M. 2001, AJ, 122, 830

Rejkuba, M., Minniti, D., Gregg, M.D., Zijlstra, A.A., Alonso, M.V., & Goudfrooij, P. 2000, AJ, 120, 801

Tonry, J.L., & Schechter, P.L. 1990, AJ, 100, 1794

Tonry, J.L. et al. 2001, ApJ, 546, 681

van den Bergh, S., & Morbey, C.L. 1984, ApJ, 283, 598

White, R.E., & Shawl, S.J. 1987, ApJ, 317, 246

Whitmore, B.C., Miller, B.W., Schweizer, F., & Fall, S.M. 1997, AJ, 114, 1797

This preprint was prepared with the AAS LaTeX macros v5.0.

Table 1. List of Individually Imaged NGC 5128 Globular Clusters

Cluster ID	α (J2000)	δ (J2000)	R_{gc} (kpc)	V	$(V-I)$	M_V	detector
C40	13 23 42.29	-43 09 39.7	24.50	18.878		-9.47	stis
C41	13 24 38.92	-43 20 08.0	24.40	18.556		-9.79	stis
C29	13 24 40.35	-43 18 06.3	22.15	17.936		-10.41	stis
G19	13 24 46.35	-43 04 12.6	9.47	19.069	1.189	-9.28	wf3
G277	13 24 47.29	-42 58 32.2	9.10	19.030		-9.32	stis
C2	13 24 51.49	-43 12 12.2	14.99	18.334		-10.02	stis
C100	13 24 51.80	-43 04 33.7	8.57	19.85:		-8.50	stis
C100	13 24 51.92	-43 04 33.8	8.57	20.08:	1.277	-8.27	pc1
G302	13 24 53.07	-43 04 35.9	8.36	19.156		-9.19	stis
G302	13 24 53.19	-43 04 35.9	8.36	19.103	1.295	-9.25	pc1
C11	13 24 54.80	-43 01 22.7	6.99	17.695		-10.66	stis
C31	13 24 57.52	-43 01 09.1	6.40	18.366		-9.98	stis
C32	13 25 03.30	-42 50 47.2	13.12	18.308		-10.04	stis
C44	13 25 31.60	-43 19 24.3	21.26	18.605	1.163	-9.75	pc1
C17	13 25 39.63	-42 56 00.7	6.50	17.612		-10.74	stis
C101	13 25 40.47	-42 56 02.7	6.53	20.342		-8.01	stis
C102	13 25 52.07	-42 59 14.4	5.65	21.431		-6.92	stis
C21	13 25 52.70	-43 05 48.1	7.60	17.769		-10.58	stis
C22	13 25 53.54	-42 59 09.0	5.98	18.143		-10.21	stis
C23	13 25 54.55	-42 59 26.8	6.06	17.191		-11.16	stis
C103	13 25 54.98	-42 59 15.4	6.22	18.880		-9.47	stis
C104	13 25 59.43	-42 55 32.2	9.40	19.957		-8.39	stis
G221	13 26 01.06	-42 55 14.8	9.88	19.203		-9.15	stis
C25	13 26 02.79	-42 56 58.3	8.92	18.333		-10.02	stis
G293	13 26 04.27	-42 55 45.4	10.00	19.122		-9.23	stis
C105	13 26 05.12	-42 55 37.0	10.25	22.006		-6.34	stis
C7	13 26 05.35	-42 56 33.7	9.64	17.104		-11.25	stis
C106	13 26 06.15	-42 56 45.4	9.66	21.280		-7.07	stis
C37	13 26 10.53	-42 53 44.0	12.56	18.342		-10.01	stis

Table 2. Measured Structural Parameters

Cluster	W_0	r_c (arcsec)	r_h (arcsec)	c	μ_V^0	ϵ	$\frac{d\epsilon}{dr}$	θ
C40	7.5	0.108	0.570	1.69	17.54	0.17	+	74^o
C41	8.1	0.042	0.322	1.87	15.91	0.05	+	174:
C29	8.1	0.064	0.492	1.87	16.00	0.11	+	92
G19	7.4	0.101	0.489	1.65	17.37	0.20		173
G277	6.9	0.067	0.248	1.49	16.53	0.05		160:
C2	8.5	0.043	0.456	1.99	16.10	0.04		82:
C100(st)	8.0	0.079	0.563	1.86	18.22	0.10		188
C100(pc)	7.5	0.093	0.464	1.67	18.04	0.11		160
G302(st)	7.2	0.052	0.231	1.60	16.38	0.14		163
G302(pc)	7.1	0.056	0.230	1.56	15.98	0.09		163
C11	8.2	0.070	0.559	1.88	15.97	0.26	−	165
C31	7.7	0.049	0.284	1.74	15.70	0.10	−	120
C32	8.8	0.030	0.389	2.06	15.75	0.06		24:
C44	7.0	0.067	0.408	1.70	16.36	0.06		160
C17	6.6	0.122	0.408	1.43	16.12	0.07		116
C101	6.5	0.110	0.345	1.38	18.60	0.09		156
C102	9.2	0.060	1.112	2.18	20.36	0.21		72
C21	8.1	0.065	0.498	1.86	15.87	0.33		33
C22	7.3	0.059	0.272	1.62	15.59	0.09	+	82
C23	7.5	0.047	0.237	1.67	14.34	0.14		60
C103	7.6	0.053	0.288	1.71	16.29	0.15	+	2
C104	7.2	0.056	0.239	1.58	17.27	0.16		57
G221	7.1	0.060	0.246	1.56	16.59	0.07		137
C25	8.2	0.053	0.447	1.90	16.18	0.13	−	100
G293	7.8	0.036	0.222	1.76	16.03	0.05		88
C105	7.2	0.191	0.809	1.57	21.60	0.18		20
C7	8.0	0.076	0.537	1.83	15.39	0.13		15
C106	6.8	0.035	0.124	1.46	17.70	0.11		25
C37	8.1	0.031	0.238	1.87	15.22	0.02		135:
±	0.6	0.006	0.010	0.15	0.20	0.07		10^o

Table 3. Clusters With Possible Extratidal Light

Cluster ID	R_{gc} (kpc)	M_V	Δb (adu)	Fraction in XT Light
C7	9.64	-11.25	12	0.11 ± 0.05
C23	6.06	-11.16	15	0.07 ± 0.04
C25	8.92	-10.02	9	0.15 ± 0.15
C29	22.15	-10.42	12	0.17 ± 0.08
C32	13.12	-10.04	10	0.15 ± 0.11
C37	12.56	-10.01	10	0.07 ± 0.09

Table 4. Estimates of Mass-to-Light Ratios

Cluster ID	σ_v (km s^{-1})	$\mathcal{L}(c)$	Υ_V ($M_\odot/L_\odot$)
C7	19.8 ± 1.3	39.56	1.45 ± 0.44
C17	20.9 ± 1.6	21.71	2.38 ± 0.71
C21	16.3 ± 2.1	41.69	1.65 ± 0.50
C23	26.1 ± 1.5	30.59	1.32 ± 0.40

Fig. 1.— Sample sections of two STIS fields, both 30″ (600 px) on a side. *Left panel:* The very luminous NGC 5128 outer-halo cluster C29 is at lower right, with a bright star at upper left. C29 has an extended envelope and a noticeably elliptical structure, $\epsilon \simeq 0.1$. *Right panel:* The bright cluster C17 is at top, a fainter cluster C101 at center, and a bright star at bottom, with other faint stars toward the right side. Notice the increased "graininess" of the background in the right panel compared with the left, which is due to the semi-resolved population of red giant stars in the halo of NGC 5128. C17 and C101 are at projected distances of only 6.5 kpc from the galaxy center, whereas C29 is 22 kpc from the center and thus has much less surrounding light from the faint halo stars. Note also that the two inner-halo clusters have more compact structures.

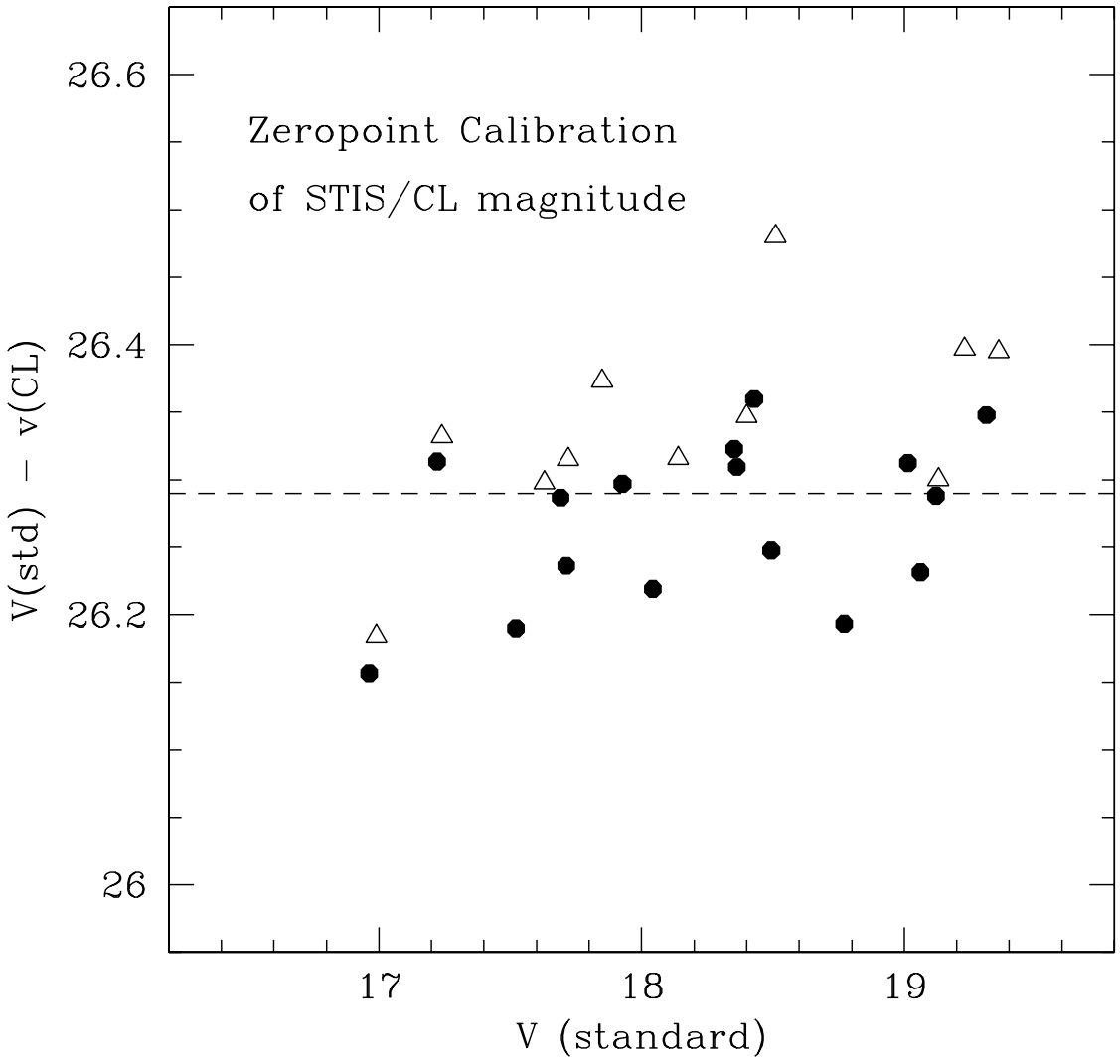

Fig. 2.— Photometric calibration of the STIS/50CCD "CL" magnitudes. Here the difference between the standard V magnitude and instrumental $v(CL)$ is plotted against V. The open triangles represent objects from the Tonry & Schechter (1990) $(V, V-I)$ data, and the filled circles are data from G.Harris et al. (1992) converted from the Washington system indices into V through Eq. (1). The dashed line is at our adopted mean of 26.29.

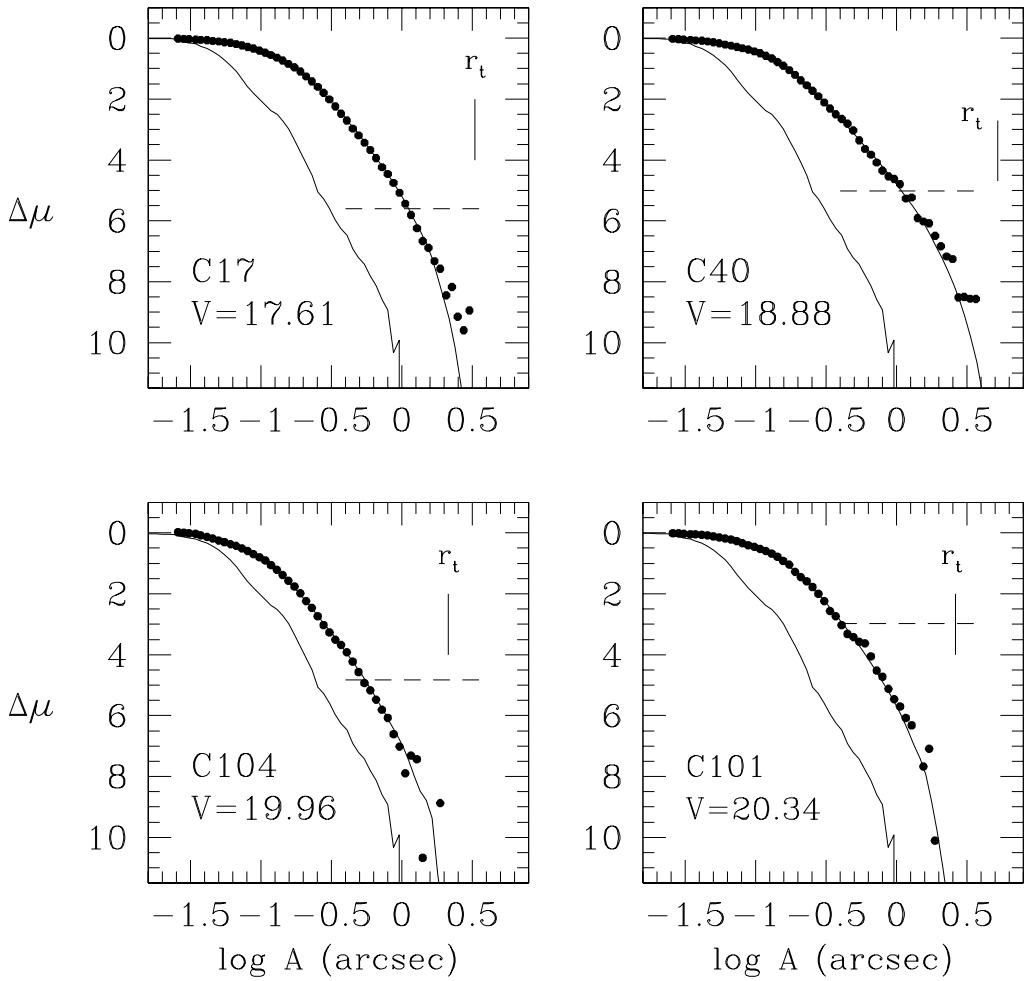

Fig. 3.— Typical profiles for four clusters imaged with the STIS camera in unfiltered 50CCD mode. Here $\Delta\mu$ is the surface intensity in V in magnitudes per unit area relative to the central surface intensity of the cluster, and A in arcseconds is the semimajor axis. In each panel, the leftmost solid line is a PSF profile for starlike objects, and the horizontal dashed line indicates the local background light intensity. Solid dots indicate the surface brightness profile determined from the *stsdas.ellipse* code, while the solid line through each data set is the best-fitting King model convolved with the PSF profile. The nominal tidal radius r_t is indicated by the short vertical line at the right edge of each panel.

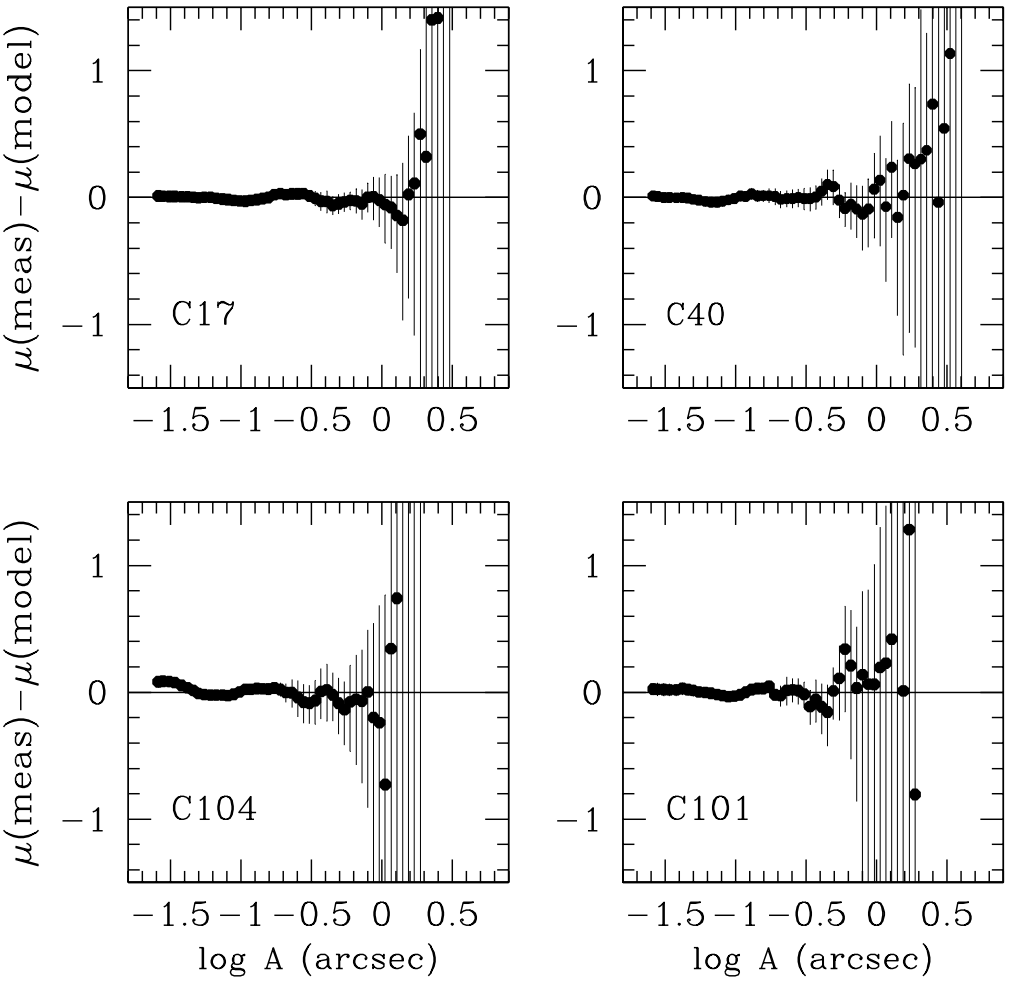

Fig. 4.— Residual light profiles (data minus model curve) for the four clusters in the previous figure. The dots represent the magnitude difference between the measured surface intensity and the best-fit King model, while the error bars show the internal uncertainty of each data point. For $\mu-$values that fall a magnitude or more fainter than the background intensity, the uncertainties rapidly blow up and exert no constraints on the fit.

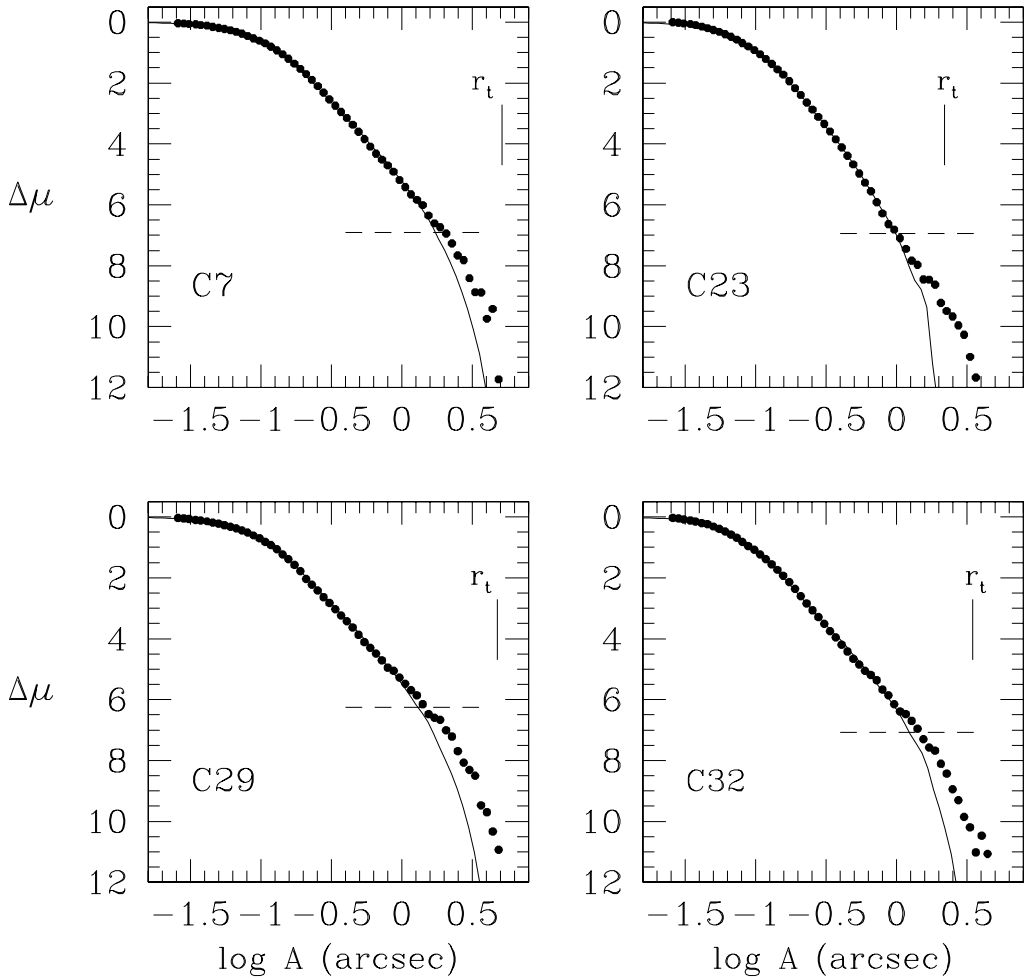

Fig. 5.— Light profiles for four clusters with possible "extratidal light" at large radii. In each panel the thin solid line represents the best-fitting King model, while the points show the actual cluster profile. The horizontal dashed line indicates the level of background light intensity for each object.

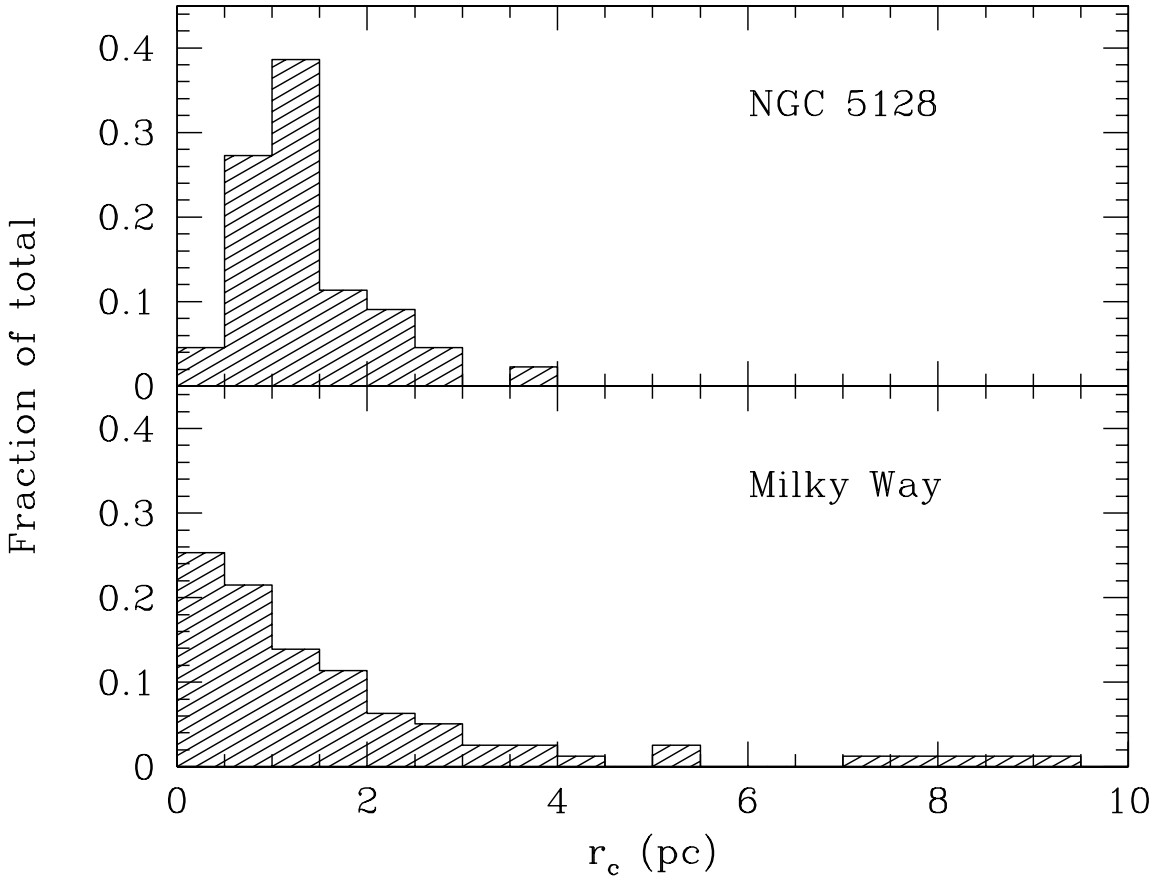

Fig. 6.— Distribution of core radii r_c of NGC 5128 clusters, compared with those in the Milky Way (see text for definition of samples). Our NGC 5128 sample lacks clusters with very small core radii, which we believe to indicate selection and measurement bias. The lack of clusters at very large r_c ($\gtrsim 5$ pc) may also be due to selection bias (see text).

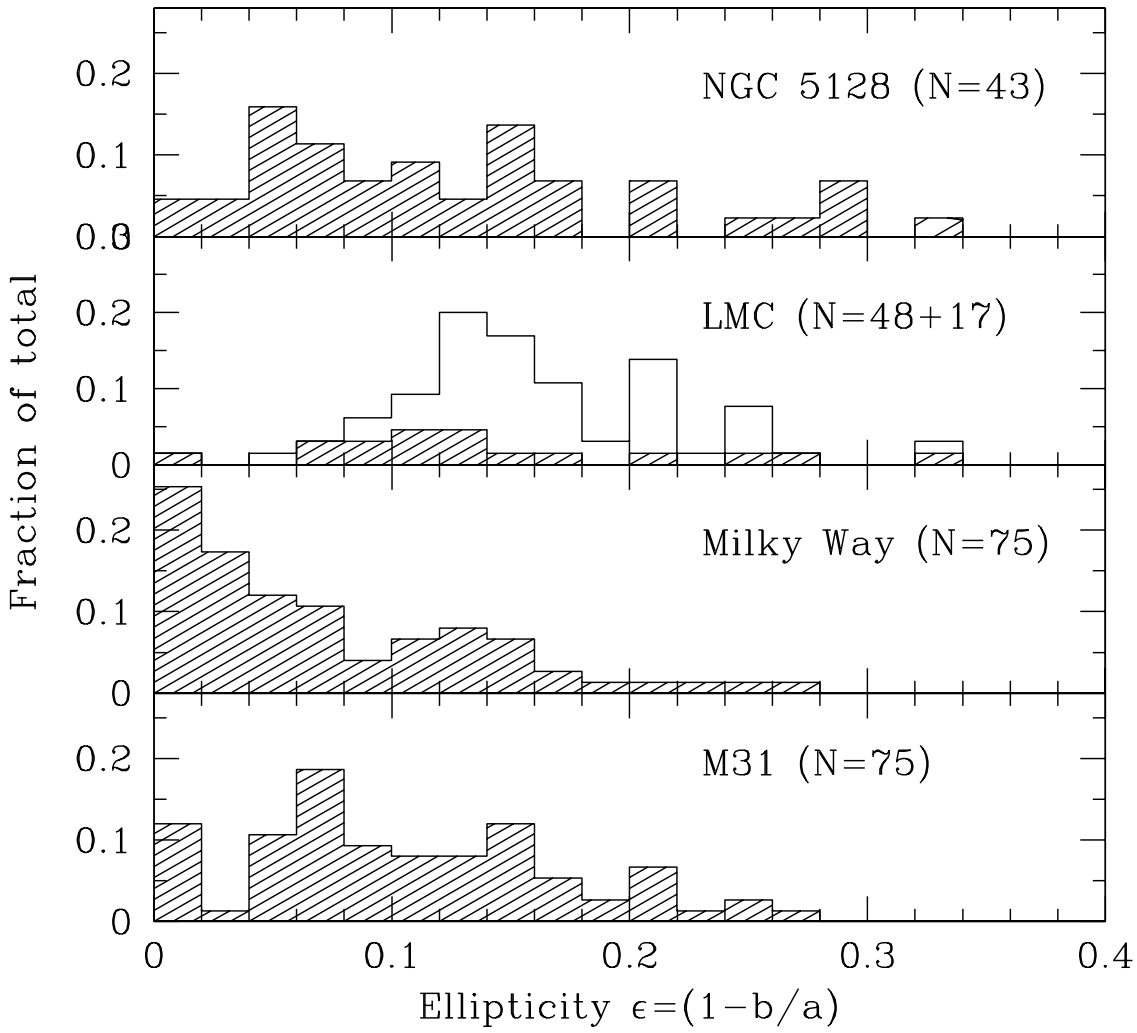

Fig. 7.— Distribution of ellipticities $\epsilon = (1 - b/a)$ for clusters in four galaxies (see text for data sources). For the LMC, the unshaded histogram is the distribution for young clusters, whereas the shaded region is for "old" clusters (SWB classes VI-VII).

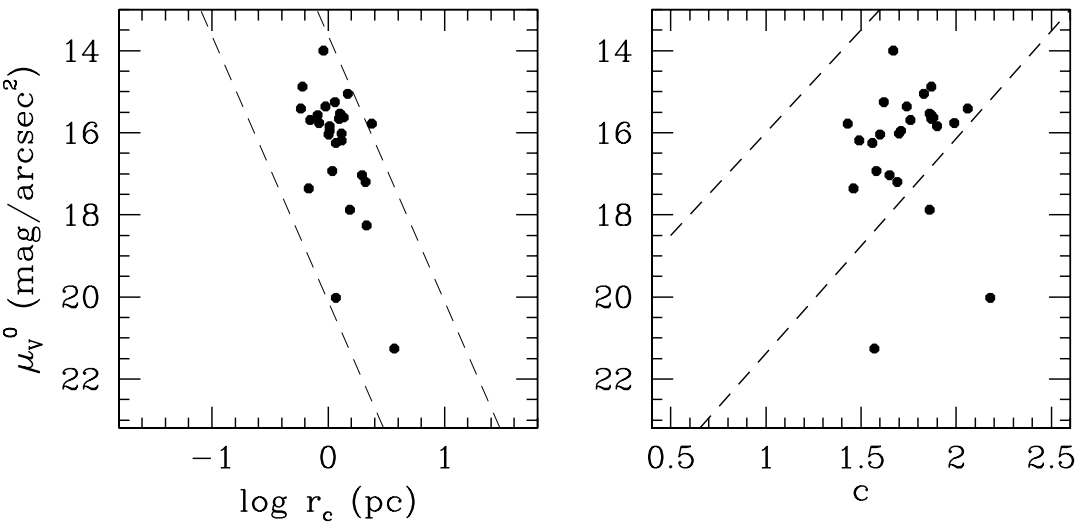

Fig. 8.— Central surface brightness μ_V^0 for our measured clusters, plotted against core radius (left panel) and central concentration (right panel). The dashed lines indicate the regions occupied by the globular clusters in the Milky Way and M31.

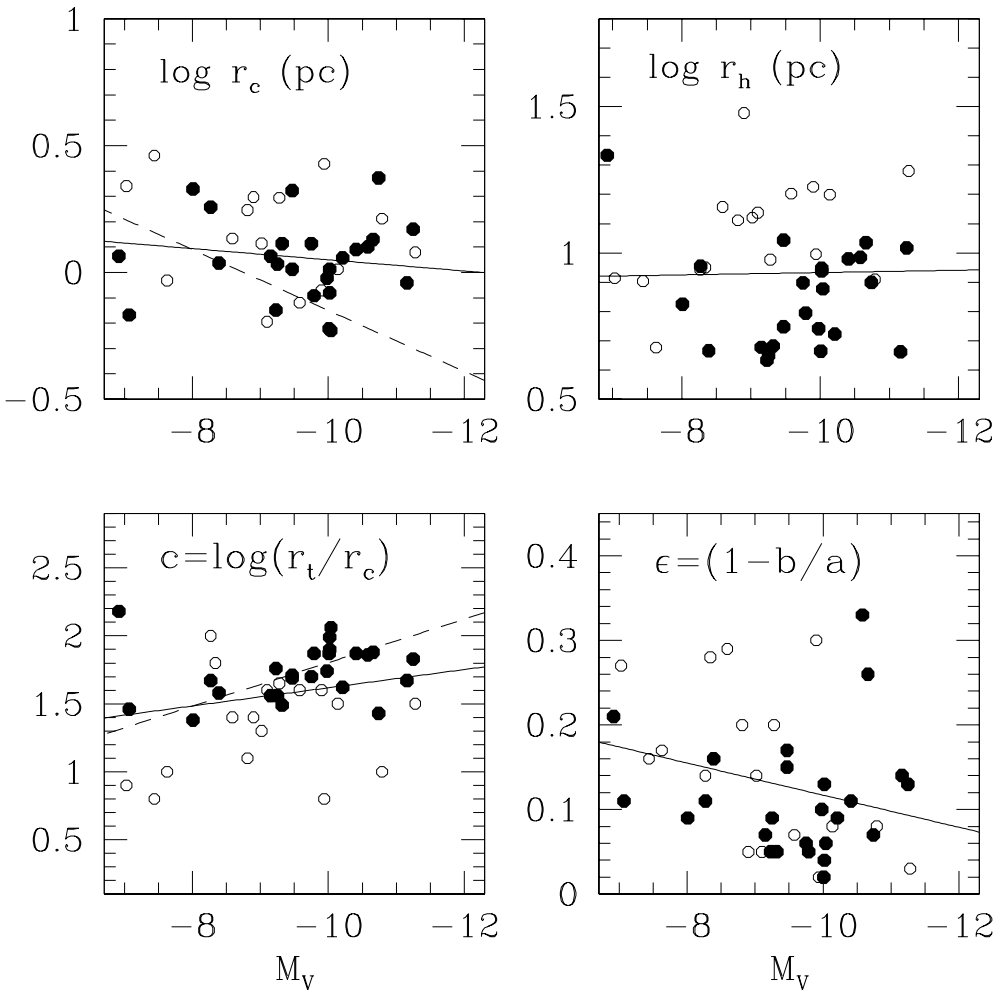

Fig. 9.— Measured structural parameters plotted against cluster luminosity. *Upper left:* logarithm of core radius (parsecs). *Upper right:* logarithm of half-light radius (parsecs). *Lower left:* central concentration c. *Lower right:* cluster ellipticity ϵ. In all the graphs, *filled circles* represent measurements from the higher-resolution STIS or PC1 cameras, while the *open circles* represent measurements from the lower-resolution WF2,3,4 cameras. The dashed lines in the two left panels are the mean relations for the Milky Way clusters, from McLaughlin (2000).

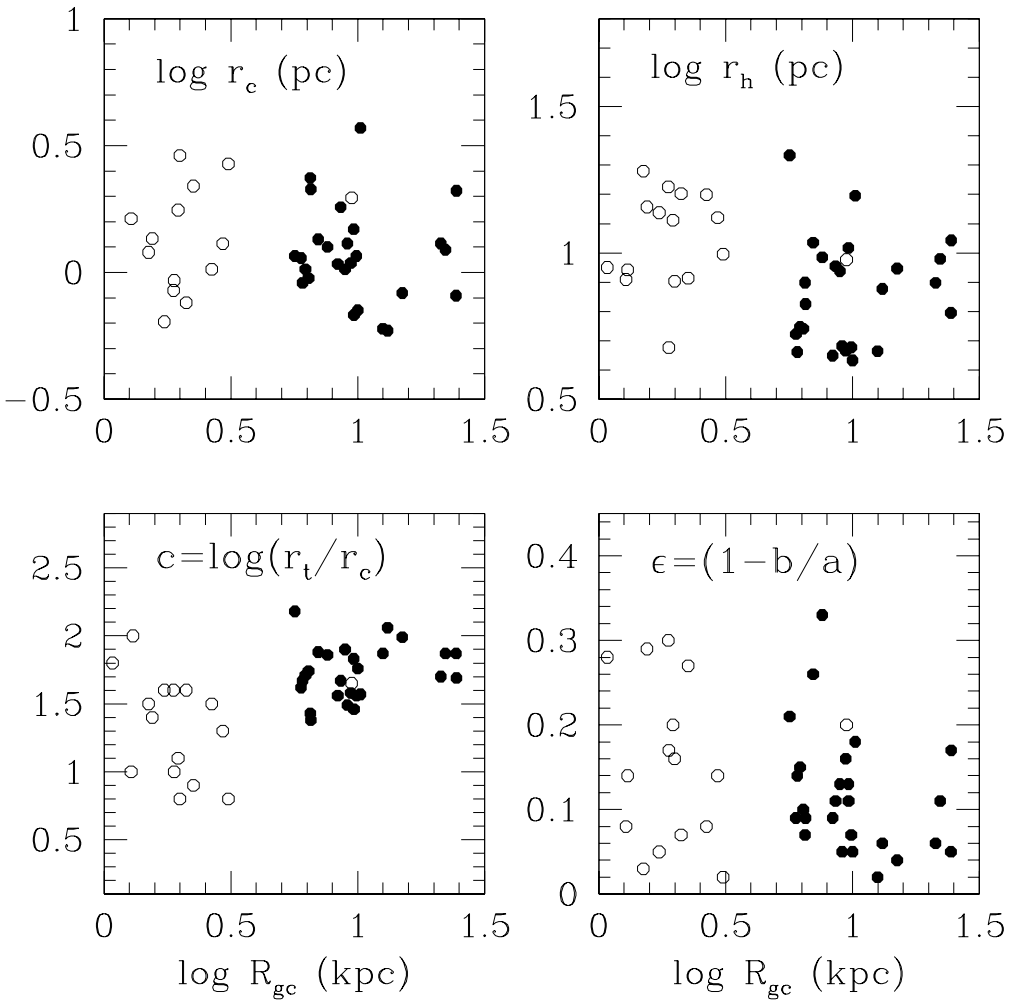

Fig. 10.— Measured structural parameters plotted against projected galactocentric distance. Symbols are as in the previous figure.

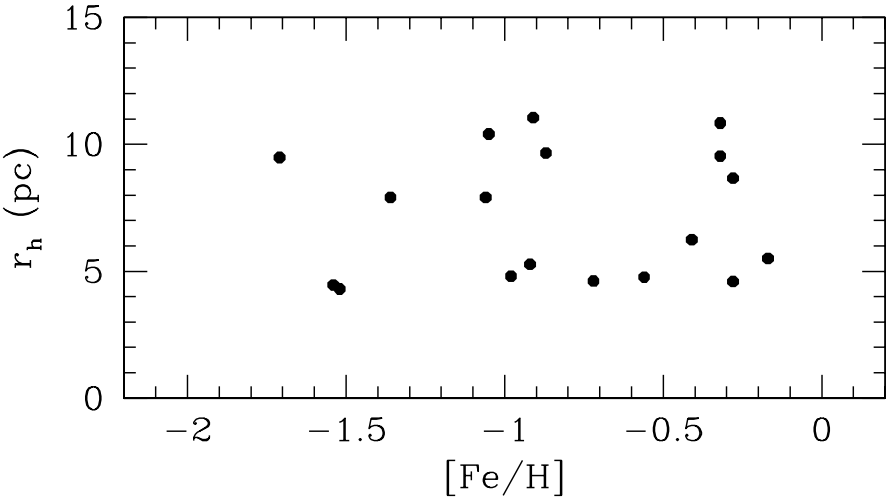

Fig. 11.— Half-mass radius r_h plotted against cluster metallicity as measured from the Washington $(C-T_1)$ photometry of Harris et al. (1992). No significant correlation is seen. Note that r_h here is expressed in parsecs, whereas in the text the least-squares fitting equation refers to r_h in arcseconds. The conversion factor used is $1'' = 19.39$ pc.

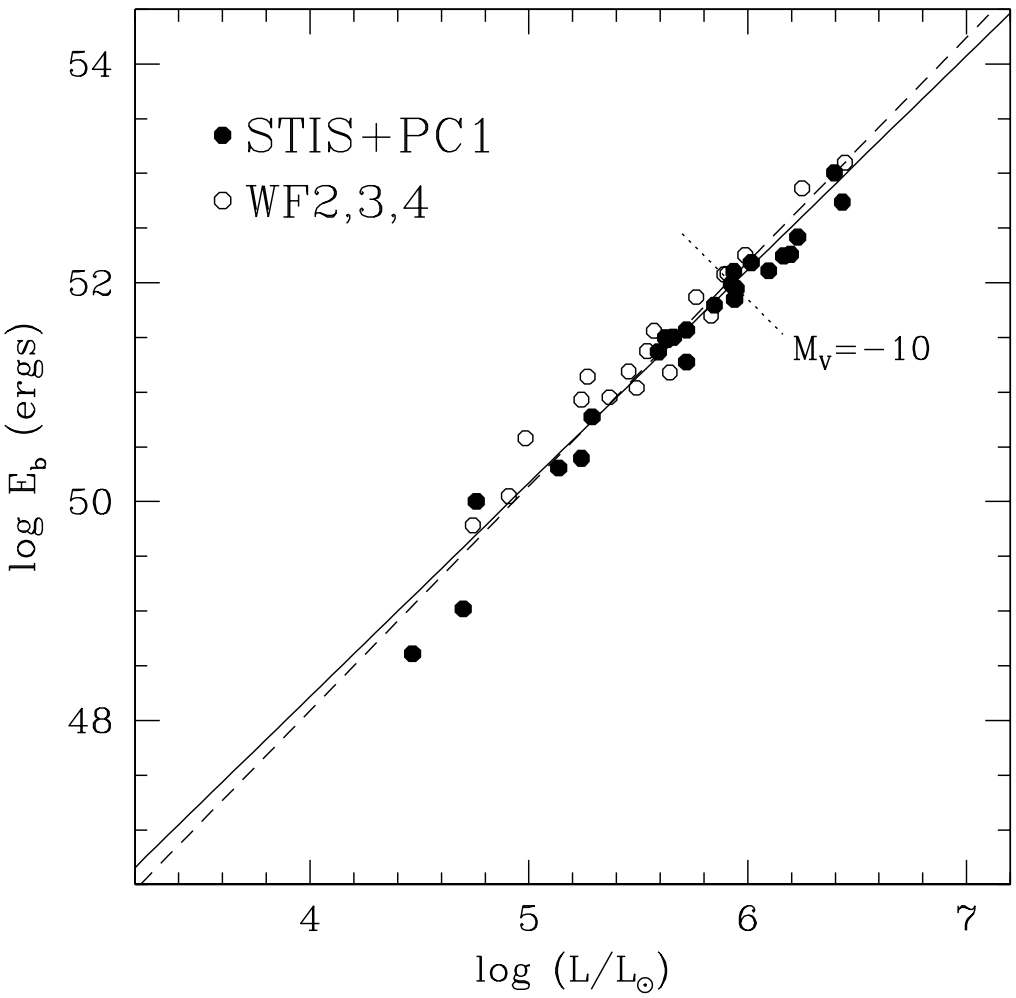

Fig. 12.— Globular clusters in NGC 5128 plotted on the plane of binding energy versus cluster luminosity. Solid dots denote clusters measured from the high-resolution STIS or PC1 detectors, while open circles denote ones measured with the lower-resolution WF detectors on the WFPC2 camera. The *solid line* is the least-squares correlation of the 43 data points shown, while the *dashed line* is the correlation obtained by McLaughlin (2000a) for the Milky Way clusters. The short dotted line marked $M_V = -10$ indicates the rough upper limit for the brightest Milky Way clusters.

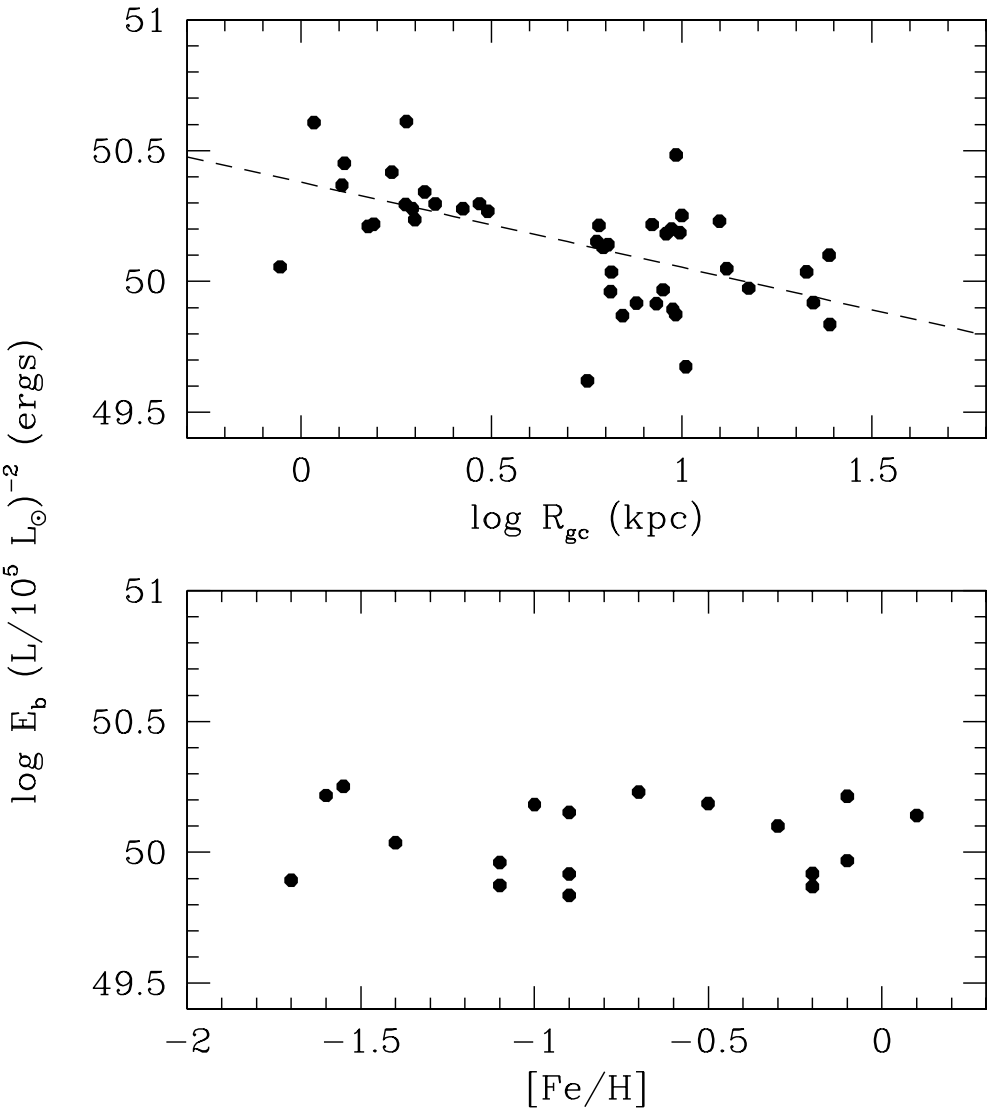

Fig. 13.— *Upper panel:* Binding energy ratio E_b/L^2, plotted against projected galactocentric distance. The dashed line gives the residual correlation $(E_b/L^2) \sim R_{gc}^{0.325}$ discussed in the text. *Lower panel:* Binding energy ratio plotted against cluster metallicity. No residual correlation is seen.

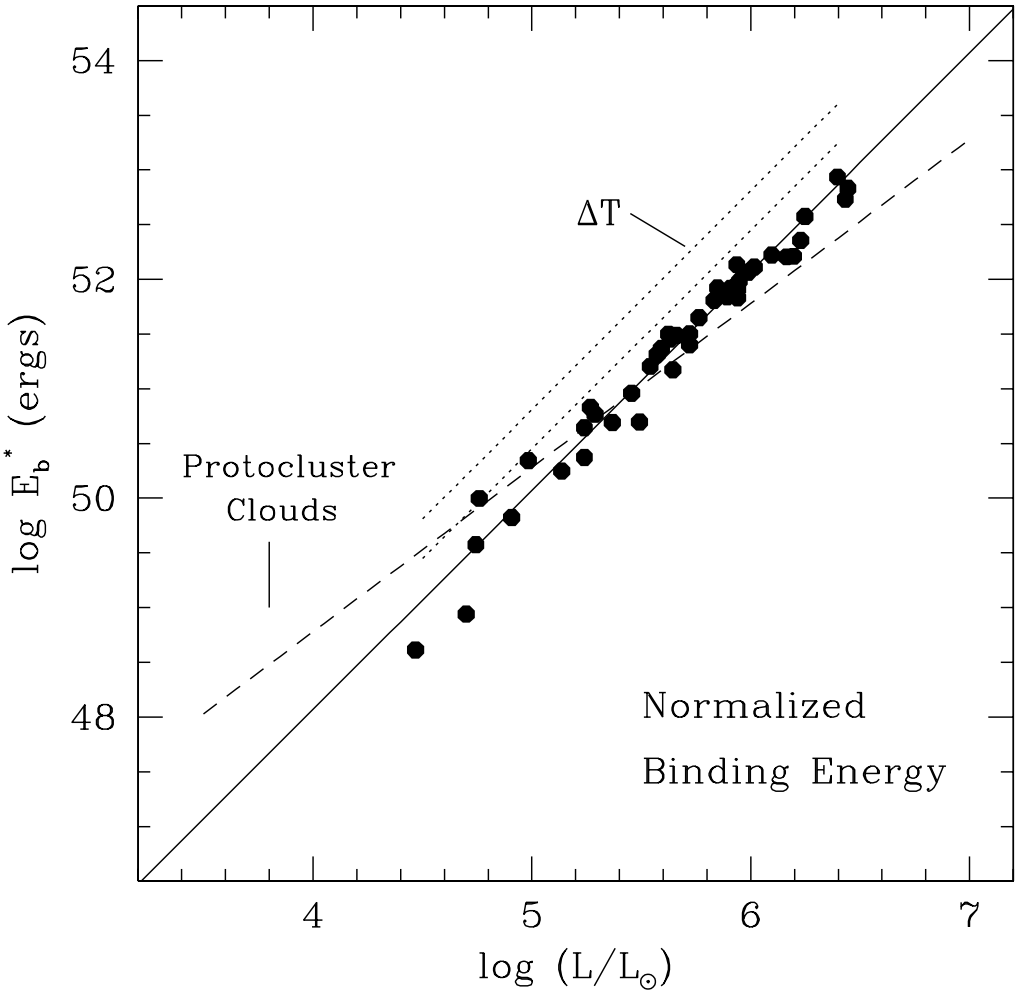

Fig. 14.— Normalized binding energy $E_b^\star = E_b \cdot (R_{gc}/10\mathrm{kpc})^{0.325}$ plotted versus luminosity. The solid line gives the least-squares relation $\log E_b^\star = 40.07 + 2.00 \log (L/L_\odot)$. The two short dotted lines above it are the loci for clusters of ages $T = 2$ Gyr (upper line) or 5 Gyr (middle line). The long dashed line is the equivalent E_b for protocluster gas clouds in an isothermal potential well at $R_{gc} = 10$ kpc and for a circular velocity $V_c = 245$ km s^{-1} (see text).

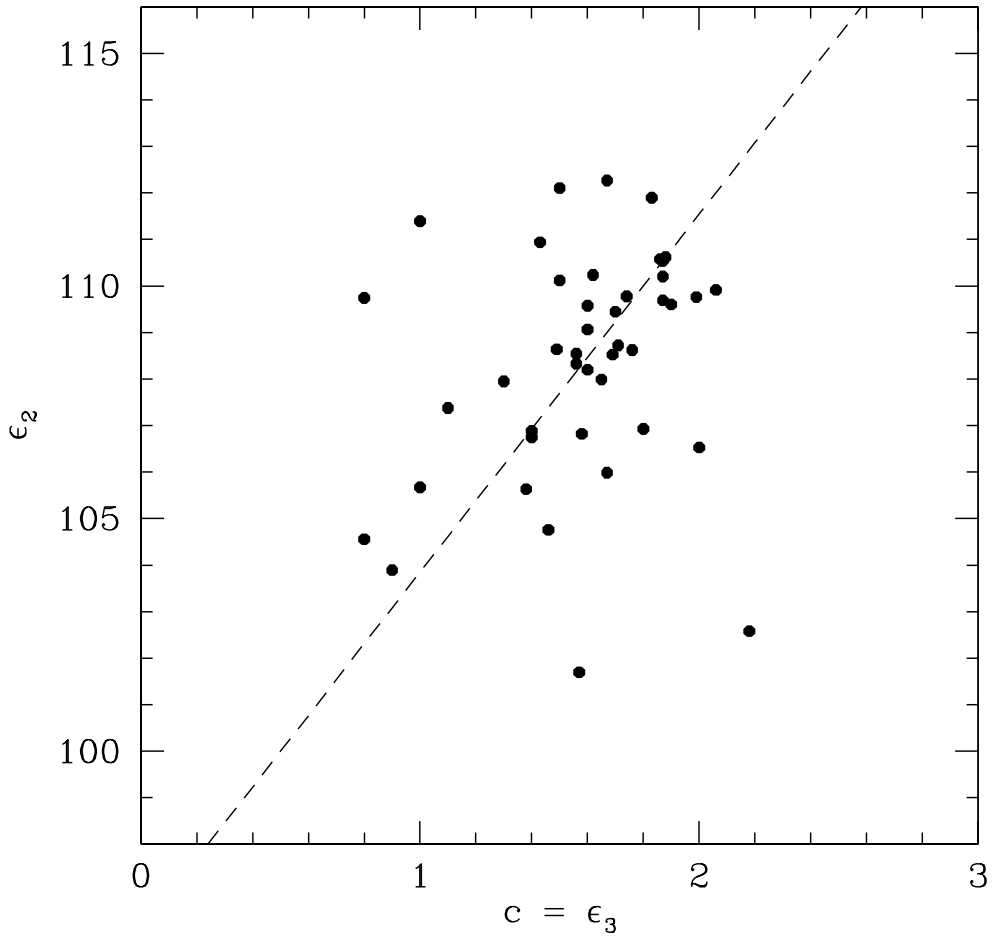

Fig. 15.— A face-on view of the "fundamental plane" for globular clusters. Here $\epsilon_2 = \log(E_b^{\star 2} \cdot L)$ as defined in the text, and $\epsilon_3 = c$. The dashed line gives McLaughlin's (2000a) relation for the Milky Way clusters, which extends to lower luminosity than we have observed here.

This figure "Harris.fig1.jpg" is available in "jpg" format from:

http://arXiv.org/ps/astro-ph/0206042v1